Acta Materialia 242 (2023) 118444

Contents lists available at ScienceDirect

Acta Materialia

journal homepage: www.elsevier.com/locate/actamat

Full length article

Finite strain crystal plasticity-phase field modeling of twin, dislocation, and grain boundary interaction in hexagonal materials

Chuanlai Liu*, Franz Roters, Dierk Raabe

Max-Planck-Institut für Eisenforschung GmbH, Max-Planck-Str. 1, Düsseldorf 40237, Germany

ARTICLE INFO

Article history:
Received 11 July 2022
Revised 13 October 2022
Accepted 16 October 2022
Available online 20 October 2022

Keywords:
Deformation twinning and detwinning
Grain neighbour effects
Plastic deformation
Magnesium alloys
Micromechanical model

ABSTRACT

Twin, dislocation, and grain boundary interaction in hexagonal materials, such as Mg, Ti, and Zr, has critical influence on the materials' mechanical properties. The development of a microstructure-sensitive constitutive model for these deformation mechanisms is the key to the design of high-strength and ductile alloys. In this work, we have developed a mechanical formulation within the finite strain framework for modeling dislocation slip- and deformation twinning-induced plasticity. A dislocation density-based crystal plasticity model was employed to describe the dislocation activities, and the stress and strain distributions. The model was coupled with a multi-phase-field model to predict twin formation and twin-twin interactions. The coupled model was then employed to study twin, dislocation, and grain boundary interactions in Mg single- and polycrystals during monotonic and cyclic deformation. The results show that twin-twin interactions can enhance the strength by impeding twin propagation and growth. The role of dislocation accommodation on twin-twin interactions was twofold. Dislocation slip diminished twin-twin hardening by relieving the development of back-stresses, while it effectively relaxed the stress concentration near twin-twin intersections and thus may alleviate crack nucleation. The plastic anisotropy in each grain and the constraints imposed by the local boundary conditions resulted in stress variations among grains. This stress heterogeneity was responsible for the observed anomalous twinning behaviour. That is, low Schmid factor twins were activated to relax local stresses and accommodate the strain incompatibility, whereas the absence of high Schmid factor twins was associated with slip band-induced stress relaxation.

1. Introduction

The formation and growth of deformation twins plays an important role in plastic deformation and ultimately in determining the formability and mechanical properties of many engineering alloys, such as Mg, Ti, and Zr alloys [1–3]. These structural alloys generally have a hexagonal close-packed (hcp) structure with fewer (easy to activate) slip systems than cubic structured materials, and a strong basal texture is usually developed during thermo-mechanical processing [4–6]. To reduce plastic anisotropy and achieve high ductility of such hcp metals, the concurrent contribution of a-axis strain from basal and prismatic $\langle a \rangle$ dislocations, and c-axis strain from pyramidal $\langle a+c \rangle$ dislocations and deformation twinning is necessary to accommodate local strain incompatibility and relax stress concentrations [2,3,7–12]. In light of this generally accepted understanding, proposed thermo-mechanical processing and alloy design strategies primarily facilitate the activation of both a-axis and c-axis deformation modes and the formation of a bimodal texture [5,13–18]. However, the intrinsic complexity of the interactions of dislocations and twins, and the strong grain neighbour effect in polycrystals creates difficulties in rationalizing the plastic deformation mechanisms and the associated mechanical behaviour.

Multiple twin variants can be activated simultaneously in a grain in hcp metals, and lead to the formation of various microstructures, such as twin-twin junctions [19–21] and double or tertiary twins [19,22]. Twin-twin junctions play a distinctive role compared to isolated twins in subsequent twinning and detwinning processes, and they are important for the development of localised stress fields. In this way, they inevitably impact the materials' mechanical properties, such as strain hardening, crack nucleation, and resistance to failure [19,23–25]. Kadiri et al. [23] reported that twin-twin interactions tended to increase the Mg $\{\bar{1}012\}$ twin nucleation rate, but hinder thickening of the individual twin lamella. The higher stress developed in grains with multiple twin variants was attributed to the formation of the

* Corresponding author.
E-mail address: c.liu@mpie.de (C. Liu).

https://doi.org/10.1016/j.actamat.2022.118444

back-stress resulting from the pile-up of twinning dislocations near twin-twin junctions, and from the Hall–Petch effect associated with twin segmentation. It was further found that twin-twin interactions can retard the detwinning process, since the dissociation of the twin-twin boundary dislocations into gliding twinning dislocations was energetically unfavorable [19,24]. Different studies have reported twin-twin interaction regions as potential sites for crack formation, resulting from the stress concentration and localization of plasticity in the vicinity of the intersected twins, *e.g.* in Mg alloys [24], twinning induced plasticity steels [26], and nickel based superalloys [27]. More recently, hierarchical twin networks have been engineered in pure Ti [28] and Mg alloys [29], respectively. It was reported that these fine twin networks led to higher strain hardening and activation of more slip systems, and thus enhanced both strength and ductility in these hcp materials [28,29]. The twin mesh configuration did not result in premature failure, but instead similar ductility has been achieved with intersected twins as without them [9,28,29]. It is envisaged that the simultaneous activation of both basal and non-basal dislocations can effectively accommodate the strain incompatibility and relax localised stress concentrations that twin-twin interaction generates. Moreover, it is reported that the distinct nanotwin architecture can even deflect or retard microcrack propagation in nanotwinned Ti [28]. Controversy thus surrounds the fundamental behaviour of twin-twin interactions, such as their ability to hinder twin growth and obstruct or transmit incoming dislocations, and the role of dislocation accommodation on the relaxation of localised stress concentrations.

The strong elastic and plastic anisotropy of the constituent single crystals and various types of orientation distributions in hcp polycrystals can potentially lead to highly localised stress fields and formation of shear bands close to grain boundaries (GBs) [30,31]. The interaction and load partitioning among grains plays a crucial role in the engineering performance of many hcp polycrystals, such as GB crack nucleation in Mg alloys [32], cold dwell fatigue in Ti alloys [33], and delayed hydride cracking in Zr alloys [34]. Furthermore, the formation of twin bands creates a new domain in the grain, usually with a hard-crystallographic orientation, and simultaneously splits the grain into two sub-grains. The progressive subdivision of grains by such hierarchical twin mesh can further enhance the complexity of load sharing among grains. In addition, the termination of twin bands or pile-ups of dislocations against GBs can result in localised stress concentrations, which can be detrimental and can induce local strain gradients, catalytic twin formation, slip transfer, formation of brittle hydrides, and crack initiation [31–36]. The extent of the localised stress and strain gradient will depend on dislocation slip types, eigenstrain of deformation twins, GB characters, and local boundary conditions. Therefore, quantitative prediction of the local stress fields and plastic deformation mechanisms associated with twin-GB and slip-GB interactions is of critical importance for understanding the relationship between the materials' microstructure, strain localisation, and crack nucleation sites.

Numerous mechanical frameworks have been developed to model the interaction of dislocations, twins, and GBs in hcp metals across multiple length scales: examples are molecular dynamics simulations of the dislocation reactions associated with twin-twin interactions in Mg [20,21]; statistical analysis on the effect of crystallographic factors on twin-twin junctions [25,37,38]; full-field crystal plasticity modeling of the heterogeneous strain and stress fields induced by slip and twin bands [39–45]; and mechanical homogenisation models for predicting the stress-strain response and texture evolution [46–49]. While crystal plasticity models provide a powerful tool to simulate the stress and strain localisation at the grain scale induced by dislocation slip, deformation twinning is usually represented as a "pseudo-slip" system using a volume fraction-based approach [50–52]. Despite being effective in describing the macroscopic stress-strain relation and texture evolution, this pseudo-slip treatment can not spatially capture the strong stress and strain inhomogeneity associated with the twin nucleation, propagation, and growth process. Explicit twin formation models have consequently been used within the crystal plasticity framework, such as direct incorporation of twin lamellae in a finite element mesh [41], explicit twin evolution with a multi-time scale subcycling algorithm [42], twin band formation by reducing the twin growth threshold stress [43,45], or introducing an interaction energy to penalize the coexistence of the matrix and twin domain [44]. However, these methods generally suffer from either the requirement for complex mesh manipulation, or poor numerical performance owing to the ill-posedness of the mechanical problem, *i.e.* the twinning induced large eigenstrain and abrupt crystallographic reorientation event [41,42]. Moreover, the occurrence of multiple twin variants and their interactions in a grain can escalate the model's complexity.

Benefiting from the diffuse interface characteristic, the phase-field method [53–62] has emerged as an effective tool to study the twinning behaviour within the micro-elasticity [63–66] and plasticity framework [39,40,67–71]. Kondo et al. [67] integrated a phase-field twinning model with a dislocation density-based crystal plasticity model, and investigated the stress relaxation and dislocation accommodation accompanying the twinning and detwinning process in a Mg single crystal. However, heterogeneous twin nucleation and propagation processes were not considered in this model, and the application was limited to single crystals [67]. In the phase-field twinning model by Rezaee-Hajidehi et al. [71], the order parameter was directly used in the logarithmic mixing rule for the interpolation of the twinning-induced strain within the diffuse interface, which ensures that twin nucleation was triggered solely by the local stress inhomogeneity. Furthermore, twinning was treated in the stretch-based kinematics, and thus two conjugate twinning systems could be represented by a single order parameter [71]. Hu et al. [69] coupled a phase-field twinning model for polycrystals with a phenomenological plasticity model to study twin-twin interactions and double twinning in Mg. However, this model was formulated in the small strain framework [69]. It is worth noting that the geometric nonlinearity related to the phase transformation and plastic deformation cannot be considered within the small strain framework. This geometric nonlinearity plays a critical role in modeling plastic processes with a large eigenstrain, such as deformation twinning, martensite transformation, and dislocation slip-induced plastic deformation. A large rigid body rotation is usually caused by the phase transformation process, and is also associated with a large eigenstrain. This material rotation does not contribute to the increase of the elastic strain energy within the finite strain framework, *i.e.* it is rotationally invariant, however, the energy and dissipation potential can be unphysically changed in a small strain linear formulation. For example, significant differences in terms of the twin morphology and stress distribution around the deformation twin in Mg have been predicted by the finite strain and small strain phase-field model [72]. Furthermore, the selection of a wrong habit plane for the growth of the deformation twin in metastable β Ti alloys was predicted using a geometrically linear formulation, while a geometrically nonlinear model can reasonably describe the anisotropic twin growth as observed in experiments [73,74].

More recently, a finite strain crystal plasticity-phase field model, that is applicable to concurrent dislocation-mediated plasticity and heterogeneous twinning behaviour in hcp materials, has been constructed by the current authors [39,40]. This model has been used to study the nucleation, propagation, and growth of $\{\bar{1}012\}$ twins, the stress relaxation effect near transverse twin boundaries, and the dislocation accommodation mechanisms within the twin and parent grain domains in Mg single- and polycrystals [39,40]. How-

ever, the model only considered a single twin variant and can not describe the simultaneous formation of multiple twin variants in one grain. The influence of twin-twin interactions on the further deformation twinning process, dislocation accommodation, development of stress and strain localisation could thus not be comprehensively investigated, which can be crucial for the mechanical performance of hcp metals.

This work therefore aims to develop a microstructure-sensitive and spatially resolved mechanical formulation capable of describing the complex twinning-detwinning behaviour, and the interaction of dislocations, twins, and GBs in hcp metals. This has been achieved by directly integrating a crystal plasticity model with a multi-phase-field model within a finite strain framework. A dislocation density-based crystal plasticity model was employed to describe the dislocation activity and spatial distribution of stress and strain fields. This plasticity model was coupled with a multi-phase-field model to simulate the propagation and growth of multiple twin variants in one grain. Accordingly, these different plastic deformation modes interact with each other through stress fields, under the local constraints applied by neighbouring grains. We begin by first describing the finite strain kinematics and the constitutive model. After developing the mechanical framework, we then systematically investigate the role of twin-twin interactions on strain hardening during the twinning and detwinning process, dislocation accommodation mechanisms accompanying twin-twin interactions, and the effect of the interplay among slip, twin, and GBs on the generation of stress concentration and strain localisation fields in Mg. Although this work focuses on the plastic deformation of Mg, the developed model can be generalised to study dislocation slip- and deformation twinning-mediated plasticity in other hcp metals.

2. Model formulation at finite strains

In this section, we formulate the coupled crystal plasticity and multi-phase-field theory for concurrently modeling dislocation slip- and deformation twinning-induced plasticity at finite strains.

2.1. Kinematics

The total deformation gradient $\mathbf{F}$ is multiplicatively decomposed into an elastic part $\mathbf{F}_e$ and a plastic part $\mathbf{F}_p$, contributed by deformation twinning and dislocation motion within the twin and parent domain, which reads as

$$\mathbf{F} = \mathbf{F}_e\mathbf{F}_p. \tag{1}$$

The evolution of $\mathbf{F}_p$ is given in terms of the plastic velocity gradient $\mathbf{L}_p$ by the flowing rule

$$\dot{\mathbf{F}}_p = \mathbf{L}_p\mathbf{F}_p, \tag{2}$$

which is driven by its work conjugate stress, *i.e.* the second Piola–Kirchhoff stress $\mathbf{S}$ in the plastic configuration.

2.2. Dislocation density-based crystal plasticity model

Following the approach of Kalidindi [50], the plastic velocity gradient $\mathbf{L}_p$ is additively composed from the dislocation slip in the parent domain, deformation twinning-induced plasticity, and the subsequent dislocation motion within the twin domain:

$$\begin{aligned}\mathbf{L}_p = &\left(1-\sum_{\beta=1}^{N_{tw}} h_{tw}^{\beta}\right)\sum_{\alpha=1}^{N_s}\dot{\gamma}_s^{\alpha}\mathbf{m}_s^{\alpha}\otimes\mathbf{n}_s^{\alpha} + \sum_{\beta=1}^{N_{tw}}\dot{\gamma}_{tw}^{\beta}\mathbf{m}_{tw}^{\beta}\otimes\mathbf{n}_{tw}^{\beta}\\ &+\sum_{\beta=1}^{N_{tw}} h_{tw}^{\beta}\left(\sum_{\alpha=1}^{N_{s\text{-}tw}}\dot{\gamma}_{s\text{-}tw}^{\alpha}\mathbf{m}_{s\text{-}tw}^{\alpha}\otimes\mathbf{n}_{s\text{-}tw}^{\alpha}\right),\end{aligned} \tag{3}$$

where $\dot{\gamma}_s^{\alpha}$ denotes the shear rate on slip system α, and the vectors $\mathbf{m}_s^{\alpha}$ and $\mathbf{n}_s^{\alpha}$ represent the slip direction and slip plane normal of the N_s slip systems in the parent grain, respectively. Slip in the twinned domain is described by the subscript "s-tw". The vectors $\mathbf{m}_{tw}^{\beta}$ and $\mathbf{n}_{tw}^{\beta}$ describe the twin direction and the twin plane normal of the N_{tw} twinning systems, respectively. h_{tw}^{β} is the twin volume fraction on twin system β at a material point. The individual dislocation slip-induced plasticity within the twin and the matrix is weighted by their respective volume fractions, as a function of the order parameter of the phase-field model. The relation between the twin volume fraction and the order parameter will be described in the multi-phase-field twinning model (Eq. (13)). $\dot{\gamma}_{tw}^{\beta} = \gamma_{ct}^{\beta}\dot{h}_{tw}^{\beta}$ is the shear rate on twin system β, where γ_{ct}^{β} and $\dot{h}_{tw}^{\beta}$ denote the characteristic shear strain and the rate of change of the twin volume fraction, respectively.

The shear rate of the mobile dislocations on a slip system is given by the Orowan equation [75] as:

$$\dot{\gamma} = \rho_m\, b\, v_0\, \exp\left[-\frac{Q_a}{k_B T}\left\{1-\left(\frac{|\tau_{eff}|}{\tau_p}\right)^{p}\right\}^{q}\right]\mathrm{sign}(\tau), \tag{4}$$

where ρ_m is the mobile dislocation density, b is the length of the Burgers vector, and v_0 is the reference dislocation slip velocity, Q_a is the activation energy for dislocation slip to overcome the obstacles, k_B is the Boltzmann constant, T is the temperature, τ_{eff} is the effective resolved shear stress as the driving force for dislocation motion, and τ_p is the Peierls stress. p and q are fitting parameters associated with the glide resistance profile.

The effective shear stress τ_{eff} is calculated as the resolved shear stress reduced by the passing stress τ_{pass}, *i.e.*

$$\tau_{eff} = \begin{cases}|\tau| - \tau_{pass} & \text{for} \quad |\tau| > \tau_{pass}\\ 0 & \text{for} \quad |\tau| \le \tau_{pass},\end{cases} \tag{5}$$

where τ is the resolved shear stress on a slip system, and the passing stress on slip system α is computed as:

$$\tau_{pass}^{\alpha} = Gb\left(\sum_{\alpha'=1}^{N_s}\varsigma_{\alpha\alpha'}\left(\rho_m^{\alpha'}+\rho_d^{\alpha'}\right)\right)^{1/2}, \tag{6}$$

where G is the shear modulus, $\varsigma_{\alpha\alpha'}$ denotes the interaction matrix between the slip system α and α', and ρ_d is the dislocation dipole density.

The evolution of the mobile dislocation density is described in terms of dislocation multiplication, annihilation, and dipole formation, *i.e.*

$$\dot{\rho}_m = \frac{|\dot{\gamma}|}{b\Lambda} - \frac{2\check{d}}{b}\rho_m|\dot{\gamma}| - \frac{2\widehat{d}}{b}\rho_m|\dot{\gamma}|. \tag{7}$$

The first term represents the generation of the mobile dislocation density due to immobilisation, and the second and third terms describe the reduction of the dislocation density due to dislocation annihilation and dipole formation, respectively. $\widehat{d}$ is the dislocation glide plane distance below which two dislocations can form a dipole, and $\check{d}$ is the glide plane distance between two dislocations below which they spontaneously annihilate. These two values are, respectively, computed as:

$$\widehat{d} = \frac{3Gb}{16\pi|\tau|}, \tag{8}$$

$$\check{d} = C_{anni}b, \tag{9}$$

where C_{anni} is a fitting parameter.

Λ in Eq. (7) represents the dislocation mean free path, describing the strain hardening behaviour, and is expressed as

$$\frac{1}{\Lambda} = \frac{1}{d_g} + \frac{\sqrt{\rho_f}}{c}, \tag{10}$$

where d_g is the grain size, and c is a fitting parameter. ρ_f is the forest dislocation density and can be calculated as

$$\rho_f^\alpha = \sum_{\alpha'=1}^{N_s} \left(\rho_m^{\alpha'} + \rho_d^{\alpha'}\right)|\mathbf{n}^\alpha \cdot \mathbf{m}^{\alpha'}|. \tag{11}$$

The evolution of the dipole density is given by

$$\dot{\rho}_d = \frac{2\widehat{d}}{b}\rho_m|\dot{\gamma}| - \frac{2\check{d}}{b}\rho_d|\dot{\gamma}|, \tag{12}$$

where the first and second terms describe dipole formation and annihilation with mobile dislocations, respectively. Thermally activated dipole annihilation is not considered in the current application at room temperature.

2.3. Multi-phase-field twinning model

In the multi-phase-field twinning model, the vector-valued phase fields $\boldsymbol{\varphi}$ are employed to describe the multiple twin variants in a grain. The order parameter at $\varphi^\beta = 0.0$ and $\varphi^\beta = 1.0$ physically corresponds to the equilibrium states of the parent and twin domain, respectively. A cubic interpolation function (see details on the comparison of the linear and cubic interpolation functions in Section S.1 of the supplementary material) is adopted to establish the relation between the twin volume fraction and the order parameter :

$$h_{tw}^\beta(\varphi^\beta) = 3(\varphi^\beta)^2 - 2(\varphi^\beta)^3. \tag{13}$$

The Gibbs free energy functional of the multi-twin system is expressed as a function of phase fields $\boldsymbol{\varphi}$, the second Piola–Kirchhoff stress $\mathbf{S}$, and the elastic Green–Lagrange strain $\mathbf{E}_e$:

$$\mathcal{F}(\boldsymbol{\varphi}, \nabla\boldsymbol{\varphi}, \mathbf{S}, \mathbf{E}_e) = \int_V \Big(f_{intf}(\boldsymbol{\varphi}, \nabla\boldsymbol{\varphi}) + f_{mech}(\boldsymbol{\varphi}, \mathbf{S}, \mathbf{E}_e)\Big)\mathrm{d}V, \tag{14}$$

where V is the domain of consideration, f_{intf} and f_{mech} represent the interfacial and mechanical free energy density, respectively.

The interface free energy density is defined as

$$f_{intf}(\boldsymbol{\varphi}, \nabla\boldsymbol{\varphi}) = \sum_{\beta=1}^{N_{tw}} \boldsymbol{\kappa}^\beta \cdot (\nabla\varphi^\beta \otimes \nabla\varphi^\beta) + \sum_{\beta=1}^{N_{tw}} \Delta f^\beta (1-\varphi^\beta)\varphi^\beta + \sum_{\beta=1}^{N_{tw}} \sum_{\beta'\neq\beta} \omega\varphi^\beta\varphi^{\beta'} + I_{[0,1]}(\boldsymbol{\varphi}) + I_{GB}(\boldsymbol{\varphi}), \tag{15}$$

where the symmetric second-order tensor $\boldsymbol{\kappa}^\beta$ is associated with the anisotropic twin interface energy. Its components $\kappa_{11}, \kappa_{22}, \kappa_{33}$ denote the gradient energy with respect to the twin tip, the lateral twin interface, and the coherent twin boundary, respectively, in the lattice coordinates. $\Delta f^\beta(1-\varphi^\beta)\varphi^\beta$ describes the crystalline energy landscape when a parent crystal is sheared into a twin crystal, where Δf^β is the height of the crystalline energy barrier to initiate deformation twinning. The third term in Eq. (15) describes the interactions between different twin variants, where a relatively large value is usually adopted for ω to prevent the coalescence of different twin variants. An indicator function on the interval [0.0, 1.0], *i.e.* $I_{[0,1]}(\varphi^\beta)$, is introduced to enforce a physical bound for twin phase fields, *i.e.* $0.0 \le \varphi^\beta \le 1.0$. It vanishes for $\varphi^\beta \in [0.0, 1.0]$ and is infinite otherwise. Furthermore, in the current work, GBs are defined to act as a rigid barrier resisting the direct transmission of deformation twins, so any twin domain in the neighbouring grain is assumed to form as a new nucleus. Hence, another indicator function $I_{GB}(\varphi^\beta)$ is introduced in the polycrystal, which is assumed to be infinite at GBs and is assigned to be zero within the grain.

The mechanical contribution to the total Gibbs free energy f_{mech}, *i.e.* the elastic strain energy density, is calculated as

$$f_{mech} = \frac{1}{2}\mathbf{S}\cdot\mathbf{E}_e, \tag{16}$$

where the elastic Green–Lagrange strain $\mathbf{E}_e$ is given by

$$\mathbf{E}_e = \frac{1}{2}(\mathbf{F}_e^T\mathbf{F}_e - \mathbf{I}). \tag{17}$$

The second Piola–Kirchhoff stress $\mathbf{S}$ is computed as

$$\mathbf{S} = \mathbb{C}\mathbf{E}_e. \tag{18}$$

A linear mixture rule is employed to calculate the average stiffness tensor $\mathbb{C}$ among different phases in a material point:

$$\mathbb{C} = \sum_{\beta=1}^{N_{tw}} h_{tw}^\beta \mathbb{C}_{tw}^\beta + (1 - \sum_{\beta=1}^{N_{tw}} h_{tw}^\beta)\mathbb{C}_m, \tag{19}$$

where $\mathbb{C}_{tw}^\beta$ and $\mathbb{C}_m$ represent the stiffness tensor for the twin system β and the parent, respectively.

The temporal and spatial evolution of the phase fields, describing the formation and growth of the deformation twins, is driven by the minimization of the total Gibbs free energy, $\mathcal{F}$, according to the generalised Ginzburg–Landau equation:

$$\begin{aligned}\dot{\varphi}^\beta &= -M\frac{\delta\mathcal{F}}{\delta\varphi^\beta}\\ &= M\Big(\mathrm{Div}\,\boldsymbol{\kappa}^\beta\nabla\varphi^\beta + \Delta f^\beta(2\varphi^\beta - 1) - \sum_{\beta'\neq\beta}^{N_{tw}} \omega\varphi^{\beta'} - \delta_{\varphi^\beta} I_{[0,1]} - \delta_{\varphi^\beta} I_{GB} - \delta_{\varphi^\beta} f_{mech}\Big),\end{aligned} \tag{20}$$

where M is the kinetic coefficient related to the twin boundary migration mobility and $\delta_x f := \partial_x f - \mathrm{Div}\ \partial_{\nabla x} f$ represents the variational derivative of f with respect to x. It is worth noting that the employment of the Ginzburg–Landau rate equation for the twin phase field renders the twinning behaviour a rate-dependent event. This rate dependence in the model can be minimised by adopting a relatively large mobility coefficient for twin interface migration compared to the strain rate used, or by formulating a mixed-type dissipation potential that combines viscous and rate-independent contributions [76]. In the current work, a large enough mobility coefficient was adopted to ensure that the overall mechanical response is mostly determined by the rate-independent threshold stress for twinning. More detail on the effect of the mobility coefficient on the twinning behaviour is given in Section S.2 of the supplementary material.

Combination of Eqs. (1)–(3) and (16)–(19) then yields the mechanical driving force for twin formation, $\delta_{\varphi^\beta} f_{mech}$, in Eq. (20), as

$$\delta_{\varphi^\beta} f_{mech} = \partial_{\mathbf{E}_e} f_{mech} \cdot \partial_{\mathbf{F}_e}\mathbf{E}_e \cdot \partial_{\mathbf{F}_p^{-1}}\mathbf{F}_e \cdot \partial_{\mathbf{L}_p}\mathbf{F}_p^{-1} \cdot \partial_{\varphi^\beta}\mathbf{L}_p. \tag{21a}$$

Assuming small elastic strain conditions compared to the twinning-induced shear deformation, this equation\ can be simplified to

$$\delta_{\varphi^\beta} f_{mech} = -\partial_{\varphi^\beta} h_{tw}^\beta \gamma_{ct}^\beta \mathbf{S}\cdot(\mathbf{m}_{tw}^\beta \otimes \mathbf{n}_{tw}^\beta). \tag{21b}$$

2.4. Numerical implementation

Restricting the attention to quasi-static processes with no external supplies of momentum, the balance relation for linear momentum is given by

$$\mathrm{Div}\ \mathbf{P} = \mathbf{0}, \tag{22}$$

where $\mathbf{P}$ is the first Piola–Kirchhoff stress, and can be calculated from the second Piola–Kirchhoff stress $\mathbf{S}$ through

$$\mathbf{P} = \det\mathbf{F}_p\mathbf{F}_e\mathbf{S}\mathbf{F}_p^{-T}. \tag{23}$$

Substituting Eq. (1)–(3), (17) and (18) through Eq. (23), into Eq. (22) yields the final linear momentum balance equations. Together with Eq. (20), these form the governing equations to be solved for the deformation fields, and the phase fields. A direct comparison of the spectral method and the finite element method for solving the phase-field and stress equilibrium equations (Eqs. (20) and (22)) was conducted in Song et al. [77], Eisenlohr et al. [78], which show that the numerical solutions from the spectral method are comparable to those from the finite element method, and both of them agree well with the analytic solutions. More detail on the comparison of these two numerical strategies is given in Section S.4 of the supplementary material. The developed mechanical model was implemented in the freeware simulation package DAMASK [52]. A large-scale parallel finite element solver using the PETSc numerical library [79] was developed to handle the discretization and numerical solution of the coupled governing equations. The self-consistent solution of the coupled fields of Eq. (20) and (22) is achieved using a staggered iteration method for each time increment. It is worth noting that the introduction of the indicator function, *i.e.* $I_{[0,1]}(\varphi^{\beta})$ in Eq. (15), yields the weak form of the Ginzburg–Landau equation, Eq. (20), in the form of a variational inequality [80,81]. This variational inequality is solved using the reduced space Newton method [80]. This results in a reduced system consisting only of the phase field degrees of freedom at twin interfaces. Therefore, the actual number of degrees of freedom to be solved in Eq. (20) is expected to be small compared to the total number of degrees of freedom of all discretization points. The numerical solution procedure is described in detail in Liu et al. [39], Shanthraj et al. [58,59].

3. Application to the plastic deformation of Mg alloys

3.1. Simulation setup

Basal $\langle a\rangle$ ($\{0\ 0\ 0\ 1\}\ \langle 1\ 1\ \bar{2}\ 0\rangle$), prismatic $\langle a\rangle$ ($\{1\ 0\ \bar{1}\ 0\}\ \langle 1\ 1\ \bar{2}\ 0\rangle$), and pyramidal $\langle c+a\rangle$ ($\{\bar{1}\ \bar{1}\ 2\ 2\}\ \langle \bar{1}\ \bar{1}\ 2\ 3\rangle$) slip systems as well as tension twins ($\{1\ 0\ \bar{1}\ 2\}\ \langle \bar{1}\ 0\ 1\ 1\rangle$) were considered to accommodate the applied deformation. The c/a-ratio was assumed to be identical to that of pure Mg, *i.e.* 1.623, which results in the characteristic twin shear γ_{ct}^{β} to be 0.129 for $\{1\ 0\ \bar{1}\ 2\}$ tension twins. Based on experimental measurements and crystal plasticity simulations on typical rare-earth-free Mg alloys, the initial threshold stresses for activating basal, prismatic, and pyramidal slip were set to be 11 MPa, 68 MPa, and 140 MPa, respectively. Since twin nucleation was not modelled as an explicit mechanism in the current work, twin nuclei were pre-inserted in all simulations. The specific geometrical configurations are given in detail in the following section together with the results. It is worth noting that, for the simulation of the plastic deformation of Mg polycrystals, multiple twin nuclei were randomly distributed along all GBs at the beginning of deformation. However, the actual twin variant selection and its subsequent propagation and growth behaviour completely depended on the development of the local stress. More detail on the comparison of the explicit with the stress-driven twin nucleation model is given in Section S.1 of the supplementary material. All geometrical models used for the current simulations were discretised with regular hexahedral elements. Since a dislocation density-based crystal plasticity model (instead of a discrete dislocation model) was used in the current work, all simulations were conducted at the meso-scale with an element size of $l_0 = 1$ μm. More detail on the mesh sensitivity of the mechanical model is given in Section S.5 of the supplementary material. The coarse elements used in the current work enabled simulations with large-scale geometries, *e.g.* 200 grains in the polycrystal setup, however, the coarse interface width in the simulation resulted in a very large twin interface energy. To guarantee reasonable simulation results in the current work, the material parameters were first benchmarked using single crystal simulations, *i.e.* the threshold stress for twin growth in the simulation was assumed to be around 27 MPa as characterised by experiments. Hereafter, these material parameters as summarised in Table 1 were used for the simulation of the plastic deformation of Mg polycrystals. Statistical comparison and assessment of the polycrystal simulations and experimental results were performed in Section 4.1. Monotonic tensile and cyclic loading under periodic boundary conditions were prescribed to the volume elements, at a strain rate of 0.001 s^{-1}.

3.2. Twin-twin interactions and detwinning

In this section, we studied cozone and non-cozone twin-twin interactions in Mg single crystals during the monotonic and cyclic deformation. A Mg single crystal containing two pre-introduced twin nuclei was used, with a domain size of 200 μm × 100 μm × 50 μm. A $(0\ \bar{1}\ 1\ 2)\ [0\ 1\ \bar{1}\ 1]$ plus $(0\ 1\ \bar{1}\ 2)\ [0\ \bar{1}\ 1\ 1]$ twin pair and a $(0\ \bar{1}\ 1\ 2)\ [0\ 1\ \bar{1}\ 1]$ plus $(\bar{1}012)\ [1\ 0\ \bar{1}\ 1]$ twin pair were considered for the case of cozone and non-cozone twin-twin interactions, respectively. The single crystal was strained along the $\langle c\rangle$ axis up to a tensile strain of 6%. In order to study the influence of twin-twin interactions on detwinning, a fully reversed strain-controlled tension–compression cycle with a strain amplitude of 5% was also imposed to the single crystal along the $\langle c\rangle$ axis.

Fig. 1 (a1–c1) show the propagation and interaction of two cozone twin variants at different tension strains. During twin propagation, strong load partitioning between the parent and the twin was observed, as shown in Fig. 1(b4) and (b5). Shear stress concentration was highly localised to the twin tips (stress level around 150 MPa) and extended out along the twin shear direction, while significant stress relaxation was observed inside the twin and the surrounding matrix (approximately at 20 MPa). Fig. 1(b2) indicates that profuse basal $\langle a\rangle$ dislocations were activated due to the high stress developed near the twin tips, although the Schmid factor for basal slip was zero. At a strain of 3% (Fig. 1(c)), these two cozone twin variants intersected with each other, leading to a large deflection of twin boundaries. The resolved shear stress and dislocation density maps in Fig. 1(c2–c5) reveal that the impingement of twin propagation resulted in localised stress concentrations within the encountering twin ahead of the incoming twin, while the stress state and basal dislocation activity in the parent domain changed dramatically from one side of the incoming twin tip to the other side. Fig. 1(d1–d5) provide information regarding the non-cozone interaction. Similarly, a high stress concentration was also observed in twin intersection regions, as shown in Fig. 1(d4) and (d5). However, both intense basal and prismatic slip (dislocation density around 3.6×10^{13} and 2.8×10^{13} m^{-2}, respectively) were activated to relax the stress concentration near non-cozone twin intersections, while only basal dislocations (around 1.9×10^{13} m^{-2}) played a pivotal role in the strain accommodation for cozone twin-twin interaction. These simulations show that both cozone and non-cozone twin-twin interactions generally come with very high local dislocation accommodation as well as stress concentration, mainly confined within the vicinity of the twin intersections, which are also susceptible to crack nucleation.

Fig. 1 (e) shows the influence of twin-twin interactions on the mechanical responses of Mg single crystals. For the single crystal with only a single twin variant, fast twin propagation resulted in a rapid stress drop from 320 MPa to 55 MPa, as shown by the black curve in Fig. 1(e). Subsequently, the twin band thickened stably at a constant applied stress of 55 MPa. When considering twin-twin interactions, the mechanical responses followed similar trends as discussed for the single twin variant. However, the applied stresses for twin growth were significantly enhanced, *i.e.* it was 80 MPa and 100 MPa at a strain of 1.5% for cozone and non-cozone twin

Table 1
Material parameters for the constitutive models.

Crystal plasticity model	b (m)	v_0 (ms^{-1})	Q_a (J)	τ_P (Pa)	d_g (m)	C_{anni}	p	q	c	$\varsigma_{\alpha\alpha'}$
Basal	3.20×10^{-10}	1.0×10^{-5}	7.0×10^{-20}	1.0×10^{7}	2.0×10^{-5}	11.0	1.0	1.0	12.0	1.0
Prismatic	3.20×10^{-10}	1.0×10^{-5}	7.0×10^{-20}	6.8×10^{7}	2.0×10^{-5}	11.0	1.0	1.0	12.0	1.0
Pyramidal	6.11×10^{-10}	1.0×10^{-5}	7.0×10^{-20}	1.4×10^{8}	2.0×10^{-5}	11.0	1.0	1.0	12.0	1.0
Twin phase-field model	$\kappa^{\beta}_{11}/l_0^2$ (Jm^{-3})	$\kappa^{\beta}_{22}/l_0^2$ (Jm^{-3})	$\kappa^{\beta}_{33}/l_0^2$ (Jm^{-3})	Δf^{β} (Jm^{-3})	ω (Jm^{-3})	l_0 (m)	M (m^3 s^{-1} J^{-1})			
	4.5×10^{8}	4.5×10^{8}	3.0×10^{7}	1.1×10^{7}	6.0×10^{7}	1.0×10^{-6}	5.0×10^{-8}			
Elastic constants	C_{11} (Pa)	C_{33} (Pa)	C_{44} (Pa)	C_{12} (Pa)	C_{13} (Pa)					
	5.93×10^{10}	6.15×10^{10}	1.64×10^{10}	2.57×10^{10}	2.14×10^{10}					

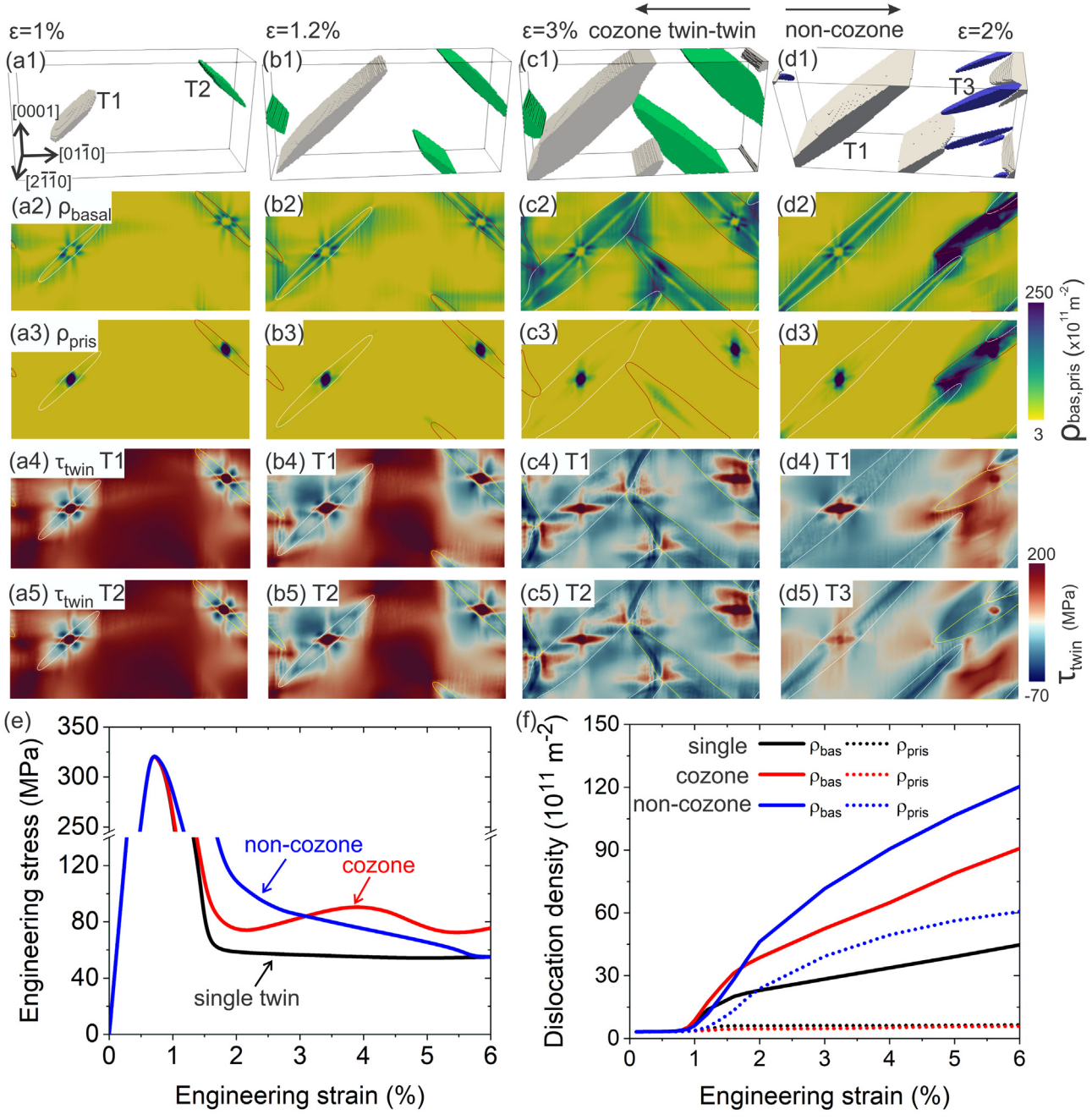

Fig. 1. Microstructure evolution and local stress distribution during cozone and non-cozone twin-twin interactions in Mg single crystals. Evolution of the twinning microstructure (a1–c1), basal (a2–c2) and prismatic (a3–c3) dislocation densities, resolved shear stress on (0$\bar{1}$12) (a4–c4) and (0 1 $\bar{1}$ 2) (a5–c5) twin systems at strains of 1%, 1.2%, and 3%. (d1–d5) provide information regarding non-cozone twin-twin interactions at a strain of 2%. (e) Simulated engineering stress versus strain curves. (f) Evolution of the average dislocation densities.

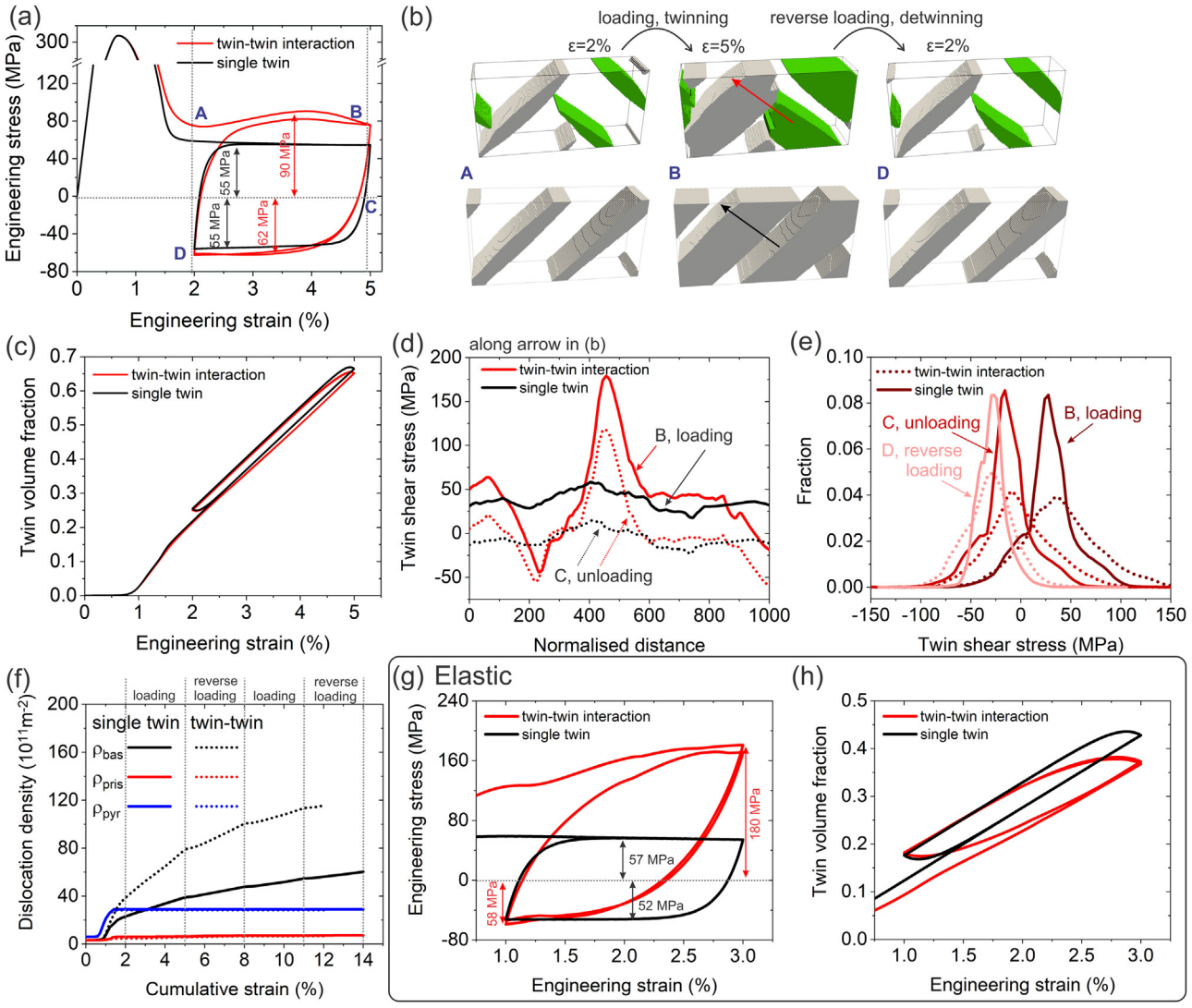

Fig. 2. Mechanical response and microstructure evolution of Mg single crystals under the cyclic deformation. (a) Stress-strain hysteresis loops with a strain amplitude of 5%. (b) Evolution of the twinning microstructure at a loading strain of 2% and 5%, and the reverse loading strain of 2%. (c) Evolution of the total twin volume fraction. (d) Variation of the twin resolved shear stress across the twin band, along the arrows in (b), at the end of tensile loading and unloading steps. (e) Frequency histograms showing the twin resolved shear stress distribution in the whole domain at the end of tensile loading, unloading, and reverse loading steps. (f) Evolution of the dislocation density as a function of the cumulative strain. The corresponding results without considering dislocation accommodation: stress-strain hysteresis loops (g) and the evolution of the total twin volume fraction (h).

variants, respectively, compared to 55 MPa for a single twin variant. This indicates that the formation of a twin network can act as a barrier to impede twin propagation yet also effectively hamper twin growth, thus producing a much higher work-hardening ability. The twin-twin hardening effect was also manifested by the enhanced activation of plastic slip, as shown in Fig. 1(f).

Fig. 2 shows the corresponding simulation results of the Mg single crystals under cyclic deformation. Fig. 2(a) shows that almost the same threshold stresses for twin growth and twin shrinkage were predicted for the Mg single crystal with a single twin variant. However, the Mg single crystal containing two cozone twin variants showed an evident Bauschinger effect during cyclic loading, *i.e.* the detwinning-induced plastic deformation occurred at a much lower stress level (62 MPa) upon reversal of the load (90 MPa). Despite producing a pronounced Bauschinger effect, the twin-twin interaction had negligible influence on the evolution of the twin volume fraction during the cyclic deformation, as shown in Fig. 2(c). Fig. 2(f) shows the evolution of the average dislocation densities as a function of the cumulative strain. It can be seen that almost no change was observed for the evolution of both prismatic and pyramidal dislocation densities during the cyclic deformation, while a gradual increase of the basal dislocation density was predicted, which mainly accommodated the deformation twinning-induced strain incompatibility. Furthermore, Fig. 2(f) shows that twin-twin interactions have significantly enhanced the activation of basal dislocations in both loading and reverse loading stages. Fig. 2(d) depicts the variation of the twin resolved shear stress across the twin band, along the arrows in Fig. 2(b), at the end of the tensile loading and unloading steps. It is clear that twin-twin interactions caused strong stress inhomogeneity within both the impinging and recipient twins. More importantly, these intense stress variations did not vanish upon unloading, although the magnitude of the stress was reduced. Fig. 2(e) presents the quantitative assessment of frequency histograms for the shear stress within the whole domain at the end of tensile loading, unloading, and reverse loading steps. It can be seen that the general shear stress distributions for all datasets at different strain states approximately followed normal distributions. At the tensile peak state, the stress distribution in the single crystal with twin-twin interactions exhibited a much larger standard deviation compared to that with only

a single twin variant, with 74 MPa compared to 36 MPa. Again, unloading and reverse loading did not alter the feature of stress variation in the domain, yet caused a shift of the average stress magnitude, depending on the applied stress. This reveals that while different plastic deformation modes controlled the deformation during loading and reversed loading, the pattern of stress heterogeneity was mainly dictated by the initial twin-twin interaction process and this pattern persisted upon unloading and reverse loading.

Fig. 2 (g) and (h) present the corresponding results of the single crystal simulation, without considering dislocation accommodation, during the cyclic deformation with a strain amplitude of 3%. Comparing Fig. 2(a) and (g), for the single crystal with a single twin variant, a similar mechanical response was predicted in the case with and without dislocation accommodation, *i.e.* twin growth and shrinkage exhibited almost the same threshold stress. However, for the case with twin-twin interactions, the single crystal without considering dislocation accommodation exhibited a much stronger Bauschinger effect than that with the activation of basal slip. For example, when dislocation accommodation was retarded, the peak loading stress was three times higher than the reverse peak loading stress (180 MPa and 58 MPa, respectively), while, when considering plastic slip, the loading stress was only about 50% higher than the reverse loading stress. The reduction of the Bauschinger effect can be ascribed to the release of the back-stress (stress partitioning between twin and matrix) within the single crystal, resulting from the activation of basal slips. Comparing the evolution of the twin volume fraction for the single crystal containing twin-twin interactions in Fig. 2(c) and (h), it can be seen that the development of the higher back-stress due to the absence of dislocation accommodation diminished the detwinning behaviour (a lower decrease rate of the twin volume fraction) during the unloading and initial reverse loading stage.

3.3. Dislocation accommodation accompanying deformation twinning

To investigate the role of dislocation accommodation in twin propagation, growth, and twin-twin interactions, two types of simulations were conducted, *i.e.* one involving both twinning- and dislocation-induced plastic deformation and another without dislocation slip. A Mg single crystal with multiple pre-inserted twin nuclei was used, with a domain size of 1000 μm × 1000 μm. It should be noted that 20 twin nuclei of the same $(0\bar{1}12)[01\bar{1}1]$ twin system were firstly introduced in the single crystal, to focus on the study of the twin propagation and growth behaviour, while two cozone twin systems, *i.e.* $(0\bar{1}12)[01\bar{1}1]$ and $(01\bar{1}2)[0\bar{1}11]$, were considered for twin-twin interactions. For simplicity, the single crystal was strained along the $\langle c\rangle$ axis up to a tensile strain of 6%. Based on the auxiliary simulations, it was found that, when dislocation accommodation was considered, the change of the loading direction (angle between the loading direction and the $\langle c\rangle$ axis from 0° to 15°) played an important role in the mechanical response, and the evolution of the twinning microstructure and basal dislocation density in the single crystal. However, when dislocation accommodation was retarded in the simulation, the loading direction only slightly affected the characteristics of the average mechanical response, local stress distribution, and the evolution of the twinning microstructure. Details on the effect of the loading direction on the twinning and plastic deformation behaviour are given in Section S.3 of the supplementary material.

Fig. 3 (a–d) show that basal dislocation accommodation, despite having a macroscopic Schmid factor of zero, played a substantial role in the morphological characteristic of tension twins. As shown in Fig. 3(a) and (c), the deformation twins without plastic slip had a nearly four times higher aspect ratio compared to the twins considering dislocation accommodation at a strain of 1.8%, being 12 relative to 3. Fig. 3(i) shows pronounced basal dislocation activity in the matrix surrounding deformation twins. More specifically, a considerable amount of basal dislocations accumulated particularly in narrow strips diagonal to the twin tip. The quantitative measurement in Fig. 4(c) demonstrates that the average shear stress near twin tips exhibited a dramatic drop from 240 MPa to 175 MPa when considering plastic slip. This implies that these basal dislocations were mainly activated to accommodate the local deformation and relax the high stress developed in the vicinity of twin tips, as shown in Fig. 3(e) and (g), which consequently decreased the driving force at twin tips and hindered fast twin propagation. Moreover, as shown in Fig. 4(c), an even more pronounced stress relaxation effect induced by dislocation accommodation was observed near twin intersection regions, namely, from 320 MPa to 170 MPa.

Fig. 4 (a) presents the influence of dislocation accommodation on the mechanical response of Mg single crystals. It can be seen that the fast twin propagation process caused sharp drop of the applied stress in all cases. However, the single crystals considering dislocation accommodation exhibited a far lower decrease rate of the macroscopic stress. As discussed above, the activation of basal dislocations led to substantial stress relaxation ahead of the twin tips (Figs. 3(e–h) and 4(c)). A sufficiently high additional stress increment must thus be imposed to facilitate further twin propagation. For the single crystals with two activated twin systems, with increasing the applied strain, twin propagation was impeded by the presence of another twin and multiple twin variants started intersecting with each other, as shown in Fig. 3(b) and (d). Subsequently, twin growth instead of twin propagation predominantly contributed to the applied plastic deformation. Fig. 4(a) reveals that the activation of basal dislocations can significantly reduce the threshold stress for twin growth, *i.e.* from 180 MPa to 140 MPa at a strain of 2.8%. This can be partially ascribed to the development of back-stresses, defined as the difference of the twin resolved shear stress between twin and matrix. The formation of twin networks would necessarily result in an additional back-stress as a result of the large strain misfit between the sheared twin and the unsheared matrix, as evidenced by the strong stress partitioning between twin and matrix in Fig. 3(f) and (h). This large back-stress would oppose the local thickening of the twin and thus provide a strong energy penalty against twin growth. As shown in Fig. 4(d), the back-stress at a strain of 1.8% was predicted to be as high as 86 MPa in the single crystal without dislocation accommodation, whereas it was only around 14 MPa when considering slip-induced plasticity.

3.4. Twin, dislocation, and grain boundary interactions in polycrystals

This section focuses on understanding the effect of the interaction between twin, slip, and GBs on the cooperative deformation of adjacent grains, and the influence of grain-neighbour interactions on the intragranular plastic deformation behaviour, such as anomalous slip activity and tension twin formation. The polycrystalline microstructure, with a dimension of 1500 μm × 1500 μm, included 200 equiaxed grains, as shown in Fig. 5. Given the two-dimensional polycrystal used here, two cozone twin systems, *i.e.* $(0\bar{1}12)[01\bar{1}1]$ and $(01\bar{1}2)[0\bar{1}11]$, were considered in each grain. Three-dimensional simulations of the plastic deformation of corresponding polycrystal samples will be performed in the future to investigate the role of the subsurface microstructure on the strain and stress partitioning, and microstructure evolution. Different crystallographic orientations were chosen for the grains ensuring that the twinning direction in all grains was confined to the $Y-Z$ plane. Multiple twin nuclei were randomly distributed along all GBs at the beginning of deformation. However, the actual twin variant selection and its subsequent propagation and growth behaviour completely depended on the development of the local stress. It is worth noting that the twin nucleus density along

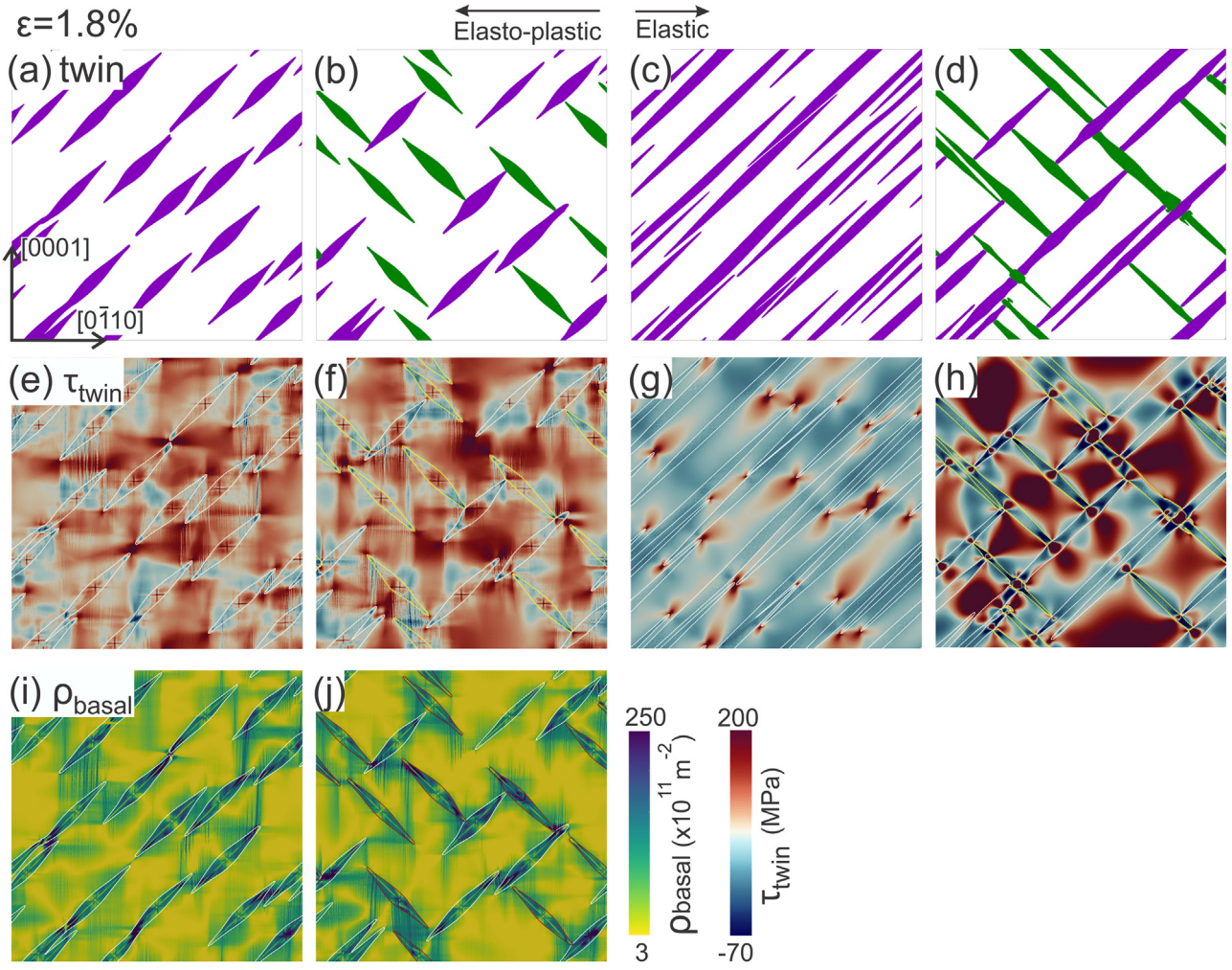

Fig. 3. Effect of dislocation accommodation on the deformation twinning and stress distribution in Mg single crystals with and without twin-twin interactions. Twinning microstructure (a, b), and the distribution of the twin resolved shear stress (e, f) and the basal dislocation density (i, j) when considering dislocation slip. (c, d) and (g, h) show the results without considering dislocation accommodation.

GBs was high enough ensuring that the propagation and growth of the activated twin variants controlled the overall deformation twin behaviour of the polycrystal. The texture of the polycrystal is here represented by the cumulative distribution function of the Schmid factor for deformation twinning, as shown in Fig. 6(a), where roughly 60% of the grains possessed a Schmid factor for twinning larger than 0.4. An uniaxial tensile deformation under periodic boundary conditions was imposed to the polycrystal along the *Z* direction up to a strain of 11%.

3.4.1. Microstructure evolution and distributions of stress and strain

Fig. 5 (a–c) present the evolution of the twin structure in the polycrystal. After 1% strain, multiple twins started propagating from GBs or triple junctions (Fig. 5(a)) and propagated into the grain interior with further deformation (Fig. 5(b)). Subsequently, most of these twins impinged on another existing twin within the grain or on GBs, and some impinged twins promoted activation of a new twin in the neighbouring grain. After 5% strain, some of the parent grains were eventually consumed by deformation twins, whereas twin-twin interactions caused pronounced grain subdivision within some of the original coarse grains. The statistical analysis (at 5% strain) in Fig. 6(d) demonstrates that the propensity for a grain to twin gradually increased as grains became more preferentially oriented for twinning. However, around 10% of these suitably orientated grains (Schmid factor larger than 0.4) did not twin, while many grains with a Schmid factor smaller than 0.2 had twinned after 5% strain. In contrast, the anomalous twinning behaviour with low Schmid factors was not observed in the polycrystal when dislocation accommodation was suppressed, as shown in Fig. 6(d). A further study of the role of dislocation accommodation on the twinning behaviour will be presented below.

The effective strain maps (Fig. 5(e–g)) show a high level of heterogeneity in the plastic response at both the intra- and intergranular scales even at low levels of deformation (1%). Several strain localisation bands were observed to span many grains at 30° to 60° to the loading direction after 2% strain (Fig. 5(b)). Furthermore, comparison of the strain distribution maps at different macroscopic strains (Fig. 5(e–g)) shows that the intergranular deformation patterns evolved with increasing applied deformation but that their main characteristics were already established at relatively low macroscopic strains. The distribution of the activated basal, prismatic, and pyramidal dislocation densities in Fig. 5(m–q) reveals that basal slip predominantly gave rise to the formation of large deformation bands, whereas non-basal dislocations were mainly confined to the region near GBs to accommodate the local strain incompatibility among grains.

Fig. 5 (d), (h), and (l) show the corresponding simulation results without incorporating dislocation-induced plasticity. The results show that the inhibition of dislocation accommodation can substantially stimulate twin formation, as revealed by the high

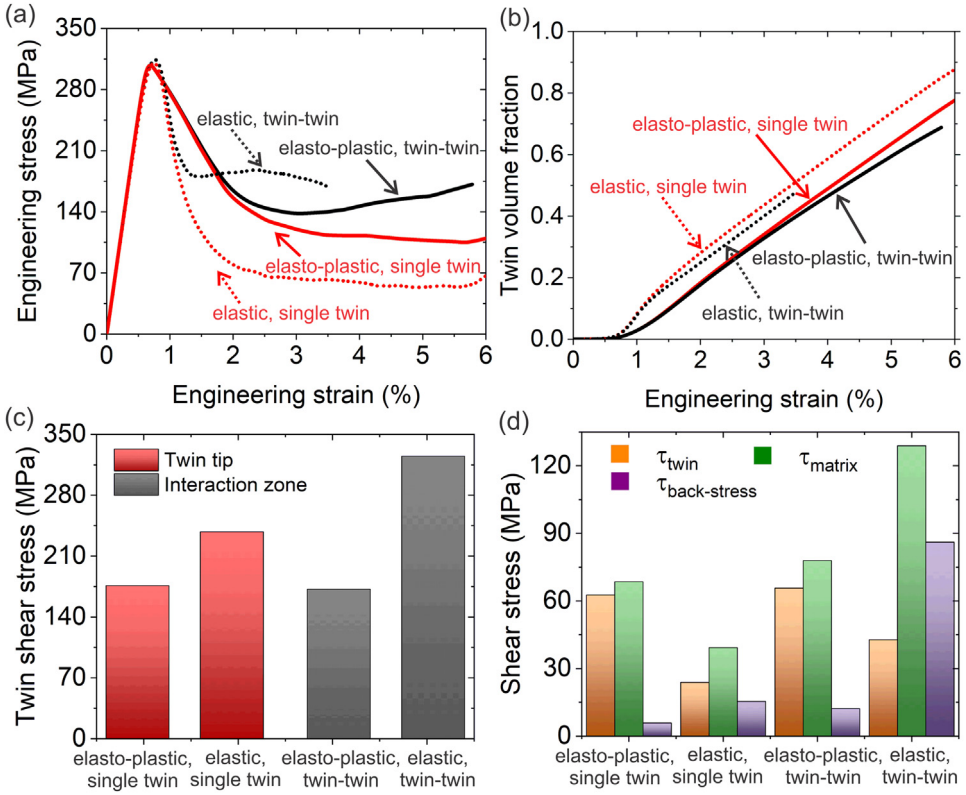

Fig. 4. Effect of dislocation accommodation on the mechanical response of Mg single crystals. (a) Stress-strain curves. (b) Evolution of the twin volume fraction. (c) The average twin resolved shear stress in the vicinity of twin tips and twin intersections at a strain of 1.8%. (d) The average twin resolved shear stress within twin and parent, respectively, at a strain of 1.8%. The back-stress is calculated as the difference of the average shear stress between twin and parent.

density of parallel twins and profuse twin-twin junctions within grains in Fig. 5(d). Since dislocation slip was retarded, the deformation incompatibility and stress concentration near GBs induced by the impingement of deformation twins can exclusively be accommodated by the activation of another twin in the neighbouring grain. This enhanced twin transmission behaviour eventually led to the formation of many large shear bands, as shown in Fig. 5(h). Furthermore, the distinctively different stress fields developed in the polycrystal with and without consideration of plastic slip (Fig. 5(i–l)) also reflect the essential role of dislocation accommodation in deformation twinning. As shown in Fig. 5(i), at 1% strain, considerable shear stress relaxation can be observed within the large slip bands. These stress relaxation zones remained in the polycrystal even when the strain was increased to 5%, as shown in Fig. 5(k), which eventually hampered the formation of deformation twins within these grains. In contrast, when dislocation slip was not available, a moderately higher shear stress developed in these grains and subsequently triggered intense twin formation (Fig. 5(d)).

Fig. 6 (b) shows the effect of dislocation accommodation on the mechanical responses of the polycrystal. When plastic slip was not considered, the rapid drop of the applied stress (by around 170 MPa) at around 1.0% strain corresponded to the amount of stress relaxation induced by fast twin propagation. Subsequently, the remarkable increase of the stress at 2% strain can be attributed to both the progressive saturation of twin activation and the enhanced strain hardening caused by twin-twin interactions. In contrast, only a slight stress decrease (around 20 MPa) was observed at 1% strain when both plastic slip and deformation twinning simultaneously accommodated the applied strain. The evolution of the activity of different plastic deformation modes in Fig. 6(c) implies that basal dislocations and tension twins acted as the primary carriers of plasticity up to 8% macroscopic strain.

3.4.2. Statistical analysis at the grain scale

Fig. 7 demonstrates the quantitative correlations between the crystallographic orientation, stress magnitude, and slip and twin activity at the grain scale. As shown in Fig. 7(a–c), although the grain-averaged twin resolved shear stress was increased proportionally to the twin Schmid factor at different strains from 0.5% to 5%, there was a large scatter in the correlation even at a low strain (0.5%). As the macroscopic load entered the elasto-plastic transition regime, profuse basal dislocations were firstly activated to accommodate the applied strain (Fig. 7(d)). However, the amount of basal slip in each grain was strongly dependent on the local boundary conditions prescribed by the neighbouring grains. The large stress variation among grains with similar orientations can thus be associated to the distinctively different basal slip activities among grains. Moreover, as shown in Fig. 7(j), when dislocation slip was suppressed, an almost linear relationship was observed between the twin resolved shear stress and twin Schmid factor prior to the activation of deformation twins. To study the influence of the grain-averaged stress developed at the initial strain on twin growth during the subsequent deformation, Fig. 7(g–i) depict the variation of the twin area fraction per twinned grain obtained at 5% strain as a function of the grain-averaged shear stress at a strain of 0.5%, 1%, and 5%, respectively. It clearly shows that the twin area fraction after 5% strain was positively correlated to the initial stress state developed in the grain, however, a wide scatter in the correlation can be observed for individual grains.

Fig. 8 shows the correlation of stress in individual parent and twin domains at a strain of 5%, corresponding to the twin growth stage. In Fig. 8(a), a wide distribution of shear stress, varying between -10 MPa and 105 MPa, was observed within both parent and twin domains. However, the average resolved shear stress measured for twins was very close to that developed in the parent domains. The observed trends also held for the corresponding mea-

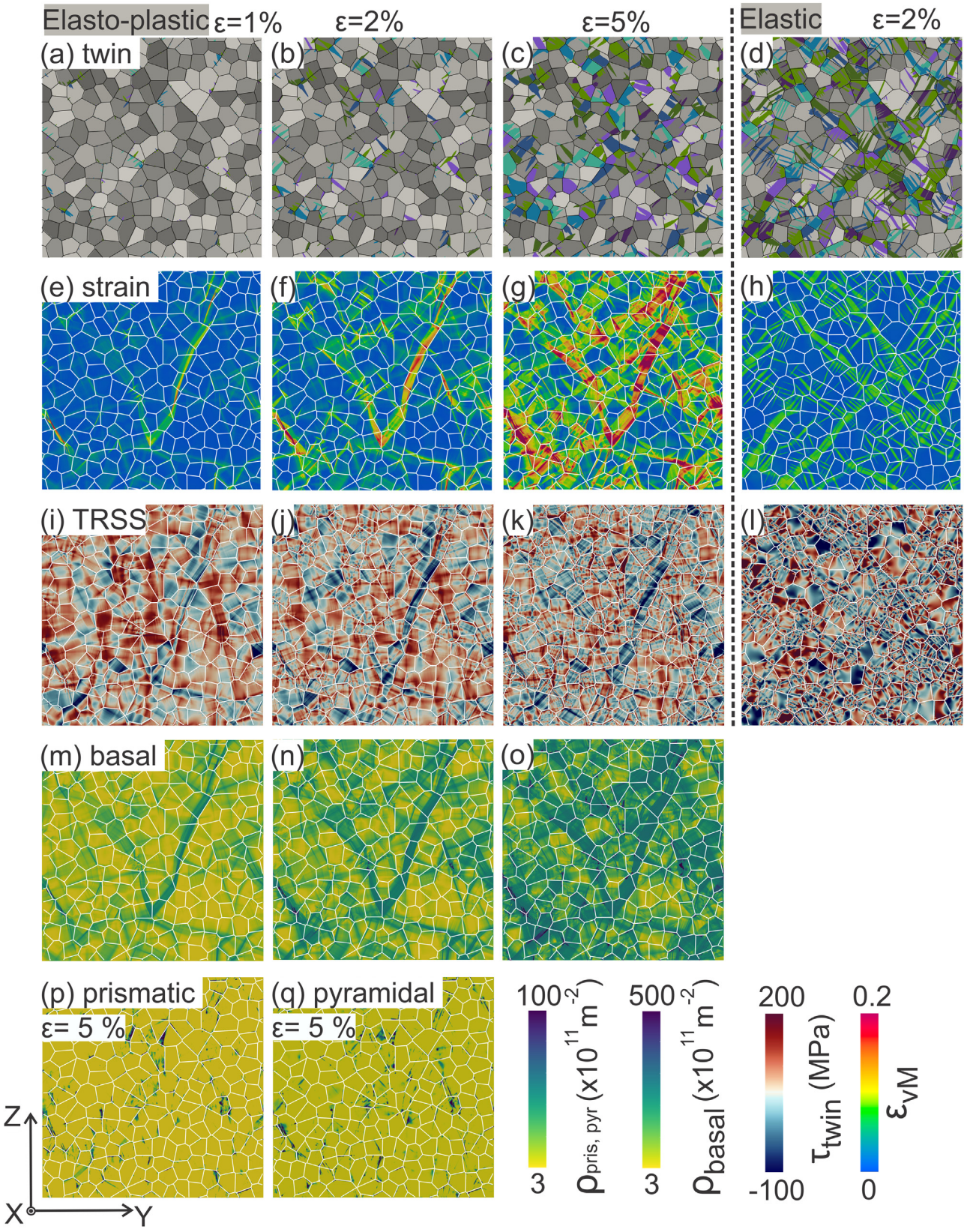

Fig. 5. Evolution of the twinning microstructure (a–c), von Mises strain (e–g), twin resolved shear stress (i–k), and basal dislocation density (m–o) of the polycrystal at a strain of 1%, 2%, and 5%, respectively. (p) and (q) showing the distribution of the prismatic and pyramidal dislocation density at a strain of 5%. (d), (h), and (l) showing the results at a strain of 2% without considering dislocation-induced plasticity.

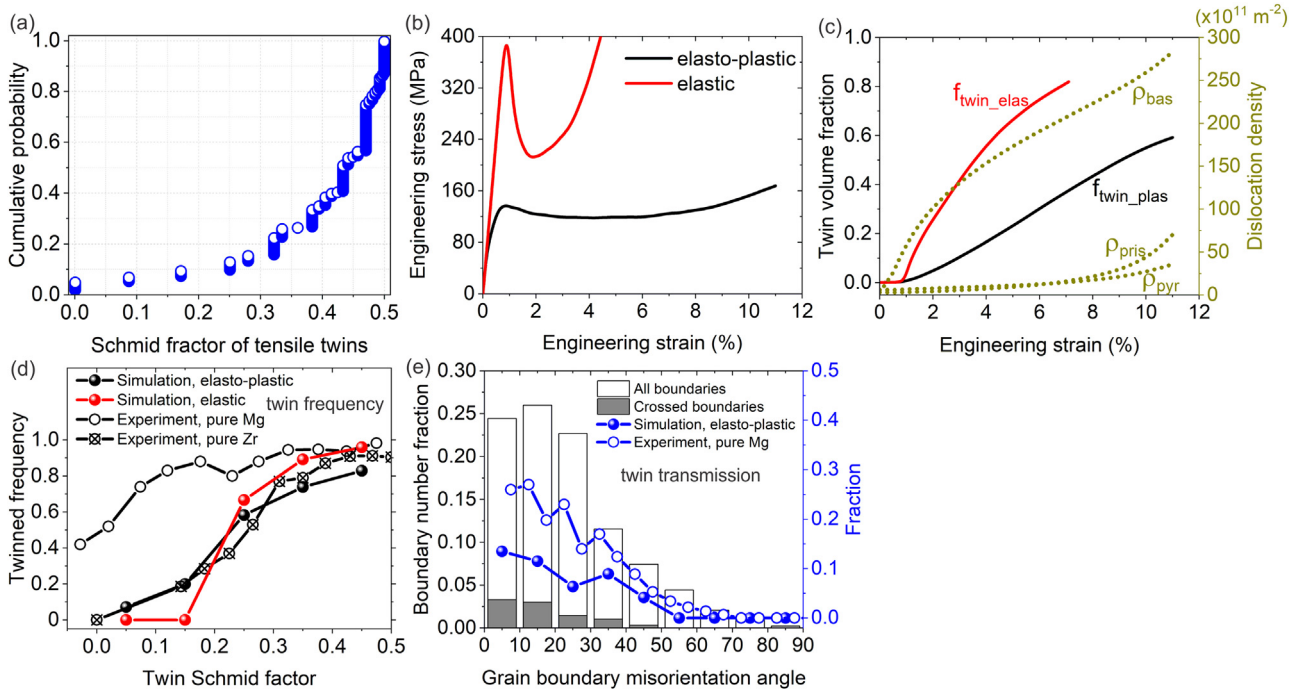

Fig. 6. (a) Cumulative distribution function of the twin Schmid factor in the polycrystal. (b) Stress-strain curves of the polycrystal with and without dislocation accommodation. (c) Evolution of the twin volume fraction, average basal, prismatic, and pyramidal dislocation densities. (d) The relationship between the twin Schmid factor and the fraction of twinned grains. The analysis with and without dislocation accommodation was performed at a strain of 5% and 2%, respectively. (e) Statistical analysis of the twin transmission frequency at GBs. White bars show the distribution of all GBs as a function of GB misorientation angle. Grey bars only include twin-crossed boundaries. Line plots show the ratios of twin-crossed boundaries to all GBs. The experimental results on pure Mg [37,82] and Zr [83] from EBSD measurements are also included in (d) and (e). The comparison and assessment of the simulations and experiments is presented in Section 4.1.

surement of the tensile stress and von Mises stress, as shown in Fig. 8(b) and (c). However, when dislocation accommodation was suppressed (Fig. 8(d)), on average, the shear stresses within twins were significantly lower than those within parents, being 20 MPa and 90 MPa, respectively. This again shows the crucial role of the basal slip activity on the relaxation of the back-stress developed within twins.

3.4.3. Stress and strain heterogeneity at the sub-grain scale

In this section, several examples of deformation localisation at the sub-grain scale are shown to investigate the role of the interaction among dislocations, twins, and GBs on the development of stress heterogeneity, and its subsequent effect on the local plastic deformation mechanism.

- **Effect of crystallographic orientation and slip activity on twin propagation:** Fig. 9(a–d) show the evolution of twinning microstructure, twin resolved shear stress, and basal dislocation density in four selected grains with twin Schmid factors ranging from 0.17 to 0.5. Fig. 9(a) and (b) show that different twin propagation behaviour was predicted in two favourably oriented grains. In both grains, tension twins were activated at 1% strain, however, the twin in one grain rapidly propagated across the whole grain with increasing deformation (Fig. 9(a)), whereas the twin in the other grain completely stopped within the grain even after a large deformation of 3% (Fig. 9(b)). Although the Schmid factor for basal slip was zero in these two grains, pronounced basal dislocation slip was activated for the grain in Fig. 9(b) after 1% strain, owing to the complex local boundary conditions. This heterogeneous basal slip activity resulted in strong stress partitioning within the grain and subsequently relaxed the driving force for twin propagation. For the grain in Fig. 9(c) with a moderate twin Schmid factor of 0.39, the competition of deformation twinning and basal slip governed the plastic deformation of the grain. For instance, the formation of a large slip band in front of the twin tip caused a substantial reduction of the shear stress for twinning and eventually impeded twin propagation. However, when dislocation accommodation was suppressed, as shown in Fig. 9(e–g), relatively high levels of shear stress for twinning evolved homogeneously within these three grains, an effect which promoted fast twin propagation across the whole grain. Finally, for the grain in Fig. 9(d) with a small twin Schmid factor of 0.17, the intense basal slip activity in the grain implies that basal dislocations were the primary plasticity carrier, whereas the twin was activated to accommodate the local deformation incompatibility near the triple junction. When dislocation slip was not considered (Fig. 9(h)), tension twins were not observed within this grain, due to the absence of local stress concentration near the GBs.
- **Basal slip mediated tension twin formation:** As shown in Fig. 10, three typical regions of interest in the deformed polycrystal were chosen to illustrate the basal slip assisted tension twin formation behaviour, with a high (0.47), moderate (0.28), and low (0.1) twin Schmid factor. After 1% strain, as indicated by the red circle in Fig. 10(a–c), profuse basal slip occurred adjacent to the newly activated twins. With increasing the strain to 2%, these small twin nuclei propagated into the interior of the grain, which was accompanied by the intensification of basal slip activity in the adjacent grain. This suggests that the activation of twins in these cases was highly stimulated by the intense basal slip activity in the neighbouring grain, especially for the low Schmid factor twin in Fig. 10(c). Fig. 10(d–f) show the results at a strain of 2% when dislocation-mediated plasticity was suppressed. For the grain with high and moderate twin Schmid factors (Fig. 10(d) and (e)), multiple twin variants were activated and connected with twins in the neighbouring grain, which can be associated with the twin

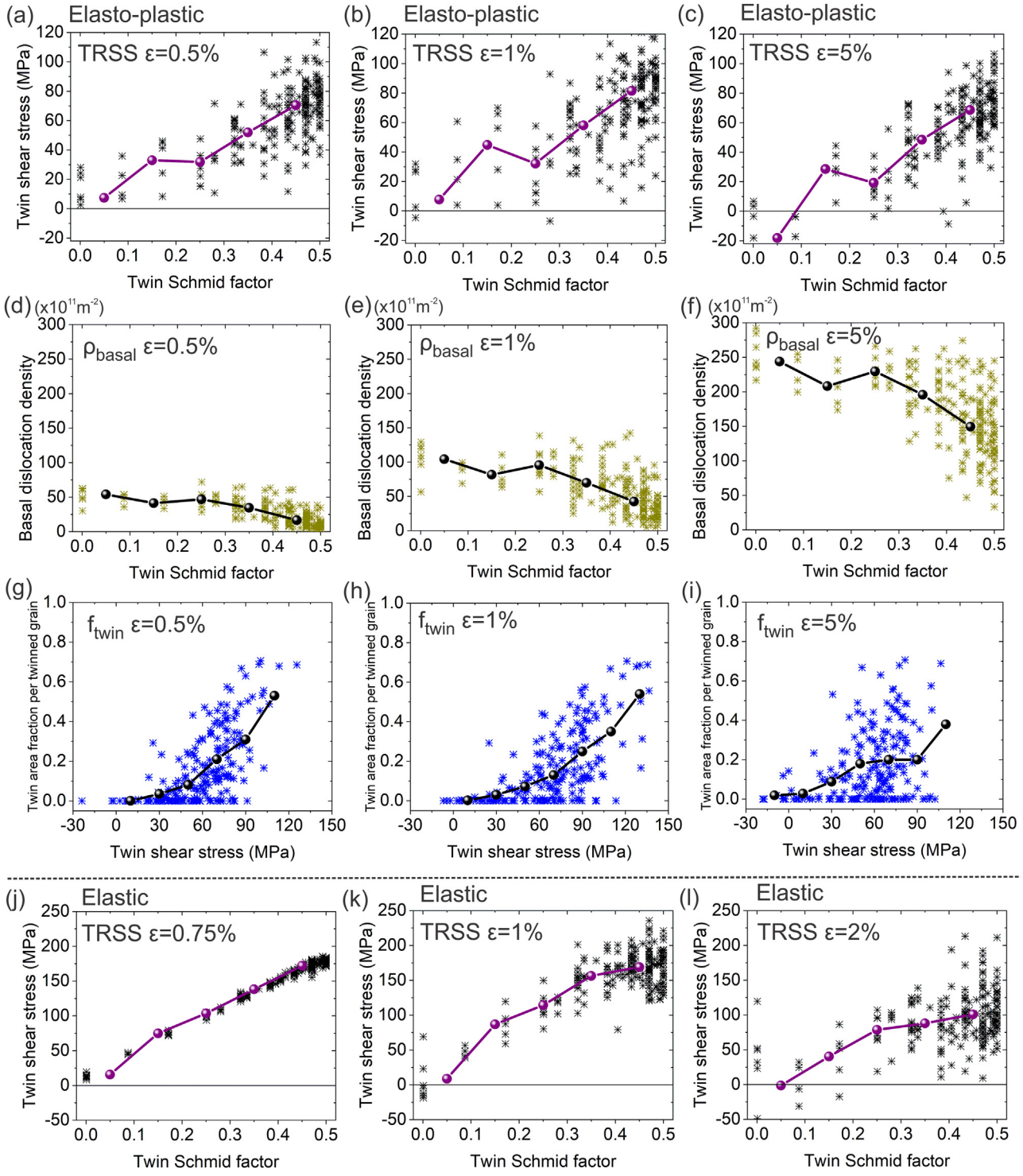

Fig. 7. Correlations between crystallographic orientation, stress, and slip and twin activity for individual grains. (a–c) Twin resolved shear stress versus twin Schmid factor. (d–f) Basal dislocation density versus twin Schmid factor. (g–i) Twin area fraction per twinned grain at 5% strain versus twin resolved shear stress at 0.5%, 1%, and 5% strains. (j–l) Twin resolved shear stress versus twin Schmid factor without considering dislocation accommodation. The solid lines show the corresponding average properties of multiple grains within each bin.

transmission behaviour across GBs. However, twin formation was not observed in the low Schmid factor grain in Fig. 10(f). This provides further evidence for basal slip assisted formation of low Schmid factor twins. Fig. 10(g–i) depict the variation in twin resolved shear stress near GBs where intense basal slip intersected the GB (along the yellow arrow in Fig. 10(a–c)). It clearly shows the localised stress concentration near GBs induced by the accumulation of basal dislocations in the adjacent grain, while the average stress within the grain interior mainly depended on the crystallographic orientation of the grain. Evidently, tension twins in these cases were activated to relax the stress concentration and accommodate the strain incompatibility caused by the intense basal slip in the neighbouring grain.

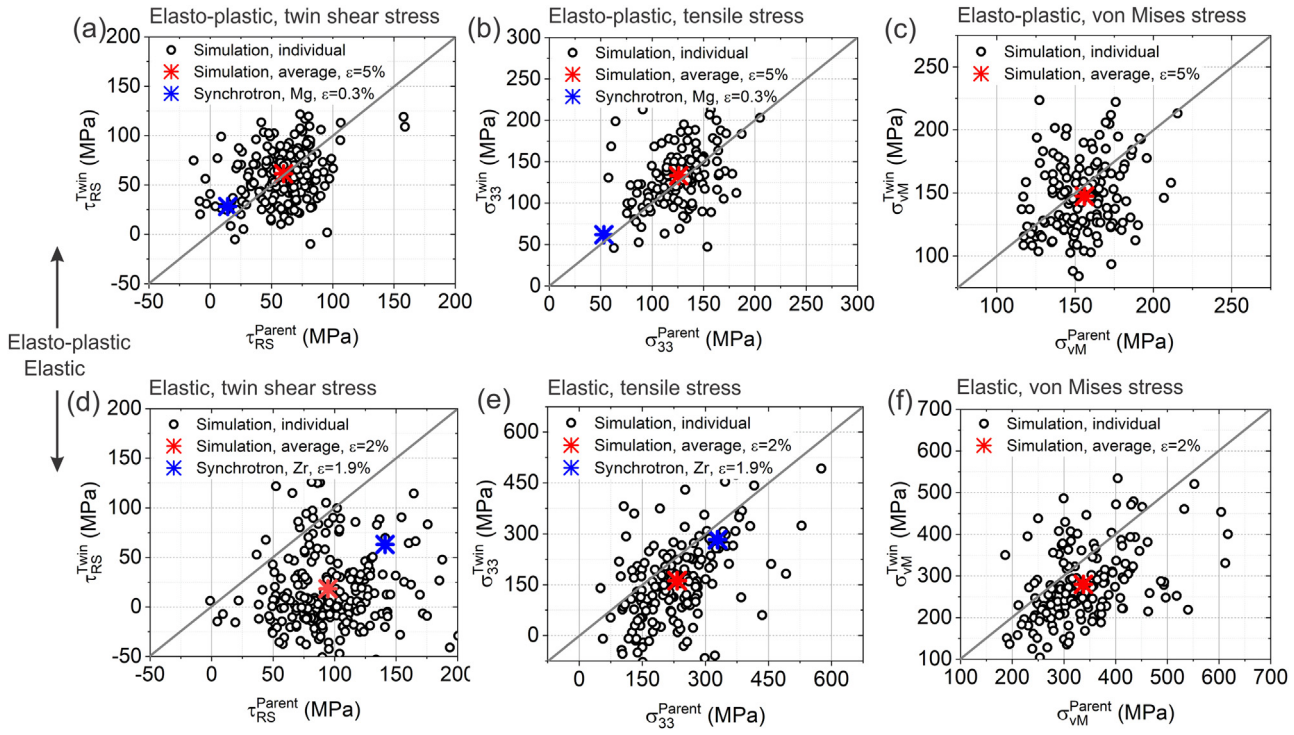

Fig. 8. Stress in the twin as a function of stress in the corresponding parent. Twin resolved shear stress (a), tensile stress (b), and von Mises stress (c) at a strain of 5%. (d–f) showing the results without considering dislocation accommodation at a strain of 2%. The asterisk symbols represents the average value for each population. The experimental results on an AZ31 Mg alloy [84] and pure Zr [85] measured by three-dimensional synchrotron X-ray diffraction are also included. The comparison and assessment of the simulations and experiments is presented in Section 4.1.

- **Retardation in the formation of twins with high Schmid factors:** Due to the anisotropic plasticity and the different local boundary conditions, the stress state in an individual grain tends to show substantial deviation from the applied stress [86,87]. Fig. 11 shows a representative region of interest in the deformed polycrystal, which demonstrates the strong grain neighbour effect on the retardation of the formation of twins with high Schmid factors. The grains with high twin Schmid factors (above 0.4), yet, without twin formation up to 5% strain were highlighted in red. Fig. 11(b) shows that these grains exhibited a relatively low twin resolved shear stress at a strain of 0.5%, although having high twin Schmid factors. The stress pattern and magnitude developed within these grains only showed subtle change with increasing the strain to 2%. In comparison, when the dislocation slip was inhibited, significantly different stress fields developed within the polycrystal (comparing Fig. 11(b) and (e)). As shown in Fig. 11(f), at a strain of 0.5%, in the case without slip-induced plasticity, the local shear stress in each grain approximately followed the trend of the macroscopic Schmid factors. However, a large deviation was observed after considering dislocation slip, *e.g.* the local shear stress in grains A, B, and C was only around 15 MPa, while it was supposed to be as high as 60 MPa based on their Schmid factors. Fig. 11(g) demonstrates that these grains with high twin Schmid factors only experienced very limited basal slip activity, therefore, the inter-grain interaction, *i.e.* the pronounced basal slip in the surrounding grains instead of the slip activity within the grain itself, was supposed to play a critical role in the development of the anomalous stress fields. Fig. 11(c) shows that grains A, B, and C were surrounded by two large basal slip bands. This means that the macroscopic strain was preferentially accommodated by their plastically soft neighbours, which caused stress relaxation and impediment of plastic deformation within the grains.

4. Discussion

4.1. Comparison and assessment of the simulations and experimental results

The application of the mechanical model in Mg single- and polycrystals in Section 3 aims to demonstrate the capability of the mechanical model, and help to understand the complex twinning-detwinning behaviour, and the interaction between twins, dislocations, and GBs in hexagonal materials at both grain and subgrain scales, rather than addressing a specific numerical simulation for a particular material scenario. Besides, some simplifications have been introduced in the current work, *e.g.* the introduction of explicit twin nuclei along grain boundaries and the two-dimensional polycrystal setup. Hence, some qualitative comparisons have been performed to assess and critically discuss the current simulations. The incorporation of a stress-driven twin nucleation method [71] and the employment of a three-dimensional polycrystal setup will be considered in future work. In Fig. 6(d), the simulated statistical relationship between the fraction of twinned grains and the twin Schmid factor was compared with the electron backscattering diffraction (EBSD) measurements on pure Mg. Both simulations and experiments reveal that the propensity for twin activation increased proportionally with an increase in the twin Schmid factor. However, the comparison indicates that the propensity to twin for low Schmid factor grains (< 0.3) observed in experiments was higher than in the simulations. As discussed in Section 3.4.1, the activation of low Schmid factor twins can be ascribed to the deviation of the local stress for a grain from the macroscopic stress. Given that Mg is elastically nearly isotropic, the highly anisotropic plastic properties and the local boundary conditions were expected to induce a substantial grain-to-grain and in-grain heterogeneity in the stress fields. Moreover, basal slip, being the easiest deformation mode in Mg, should play a distinctive

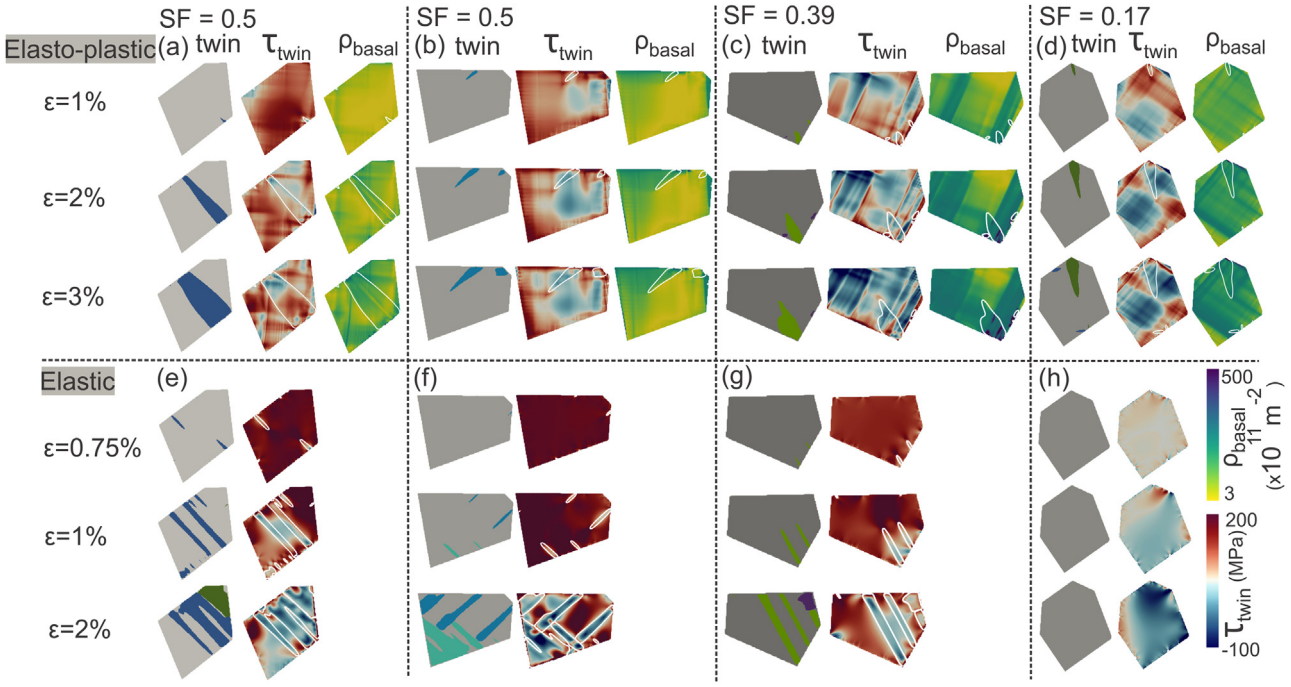

Fig. 9. Effect of crystallographic orientation and slip activity on twin propagation. Evolution of twinning microstructure, twin resolved shear stress, and basal dislocation density within the grain with Schmid factors of 0.5 (a), 0.5 (b), 0.39 (c), and 0.17 (d), respectively. (e-h) showing the results without dislocation-mediated plasticity. The location of twin boundaries was overlaid in white in the map.

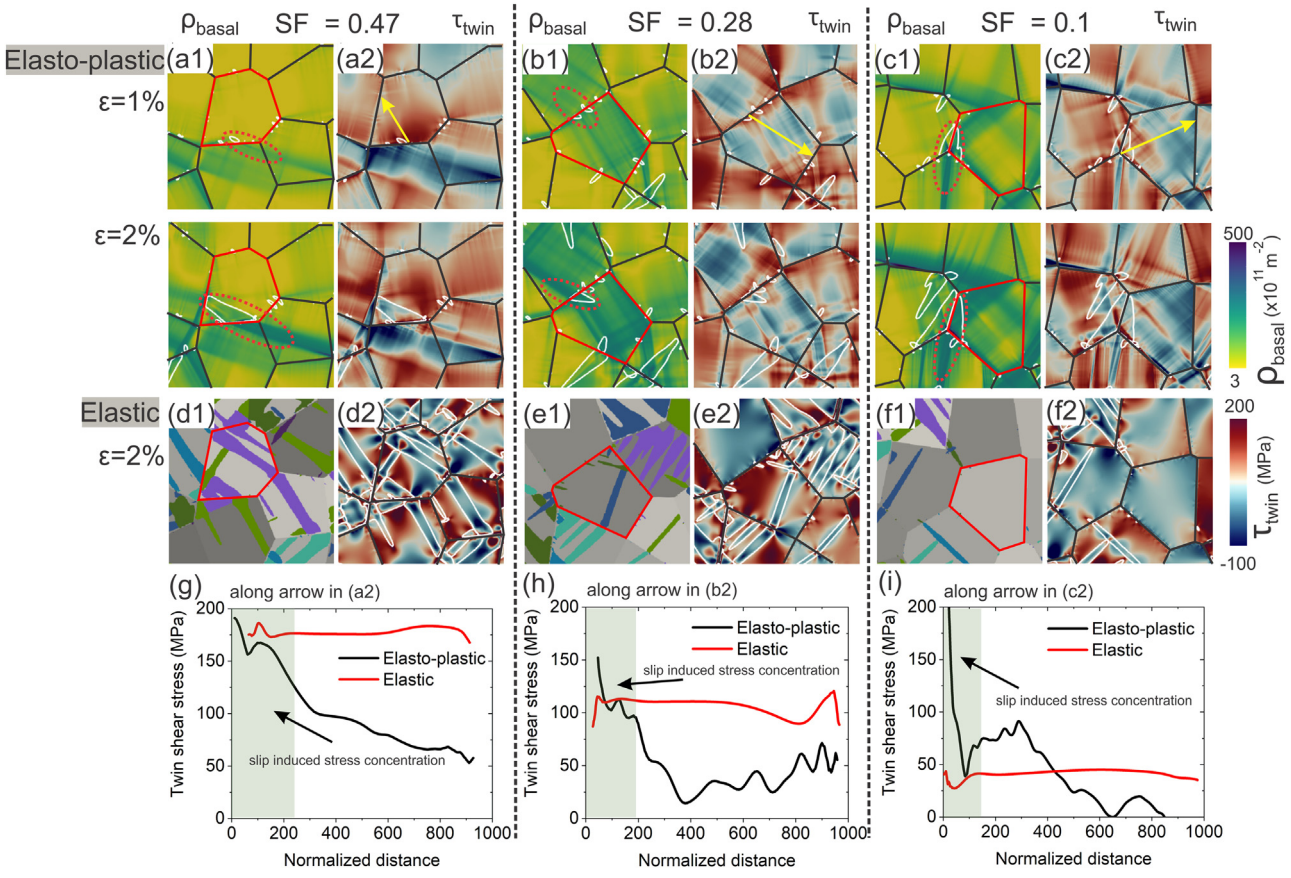

Fig. 10. Basal slip mediated tension twin formation. Distribution of the basal dislocation density (a1–c1) and twin resolved shear stress (a2–c2) within three subsets of the deformed polycrystal. The twin Schmid factor for the highlighted grain (in red) is 0.47 (a), 0.28 (b), and 0.1 (c), respectively. The location of twin boundaries was overlaid in white in the map. (d–f) showing the results without considering dislocation-mediated plasticity. (g–i) showing the variation in the twin resolved shear stress along the yellow arrow in (a2–c2) at a strain of 1%. (For interpretation of the references to colour in this figure legend, the reader is referred to the web version of this article.)

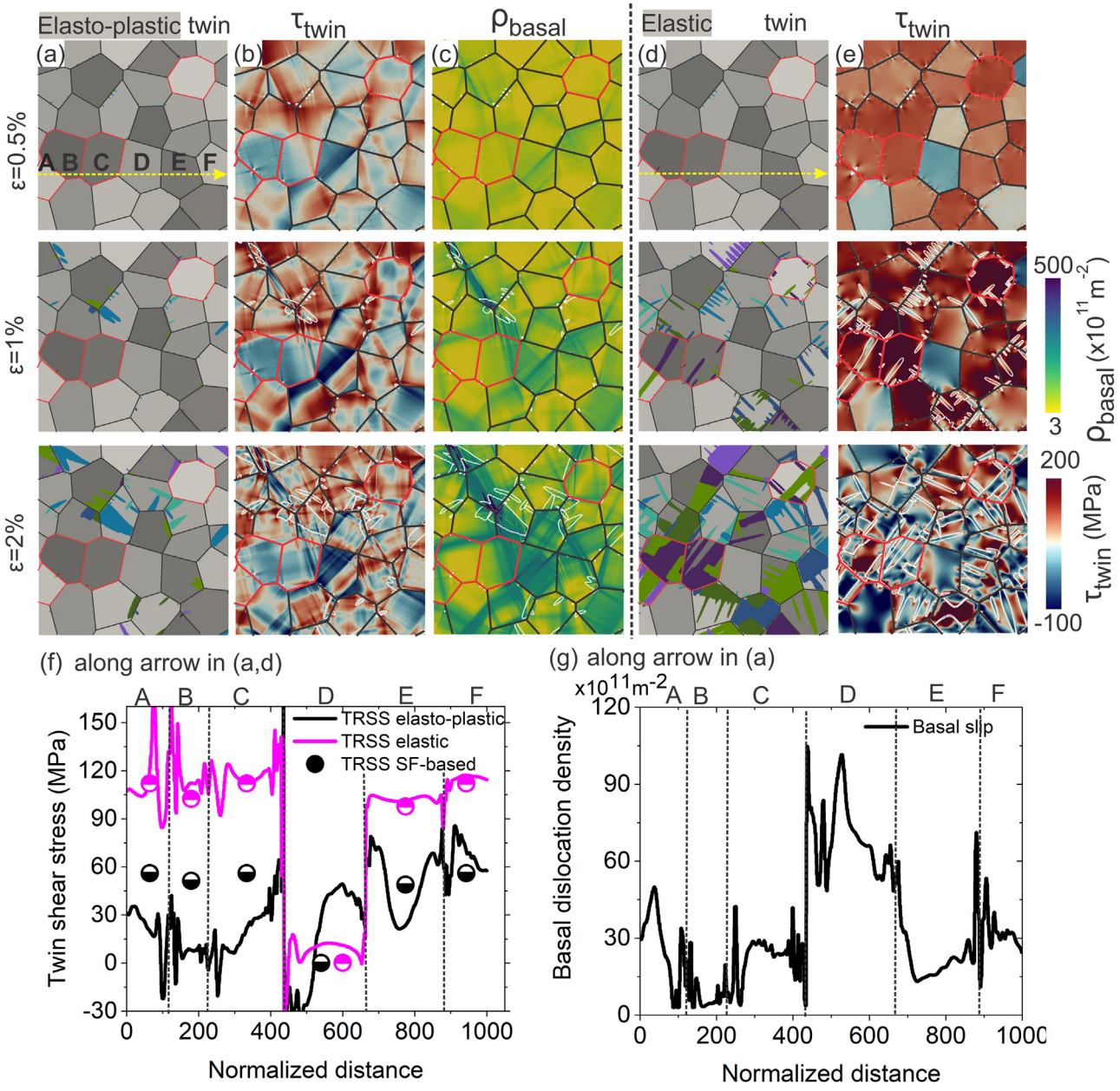

Fig. 11. Retardation of twin formation with high Schmid factors. Distribution of the twinning microstructure (a), twin resolved shear stress (b), and basal dislocation density (c) within a representative region at strains of 0.5%, 1%, and 2%. The grains with high twin Schmid factor yet without twin formation were highlighted in red. (d) and (e) showing the results without considering dislocation-mediated plastic deformation. (f) and (g) showing the variation in the twin resolved shear stress (f) and basal dislocation density (g) across multiple grains at a strain of 0.5% (along the yellow arrow in (a) and (d)). (For interpretation of the references to colour in this figure legend, the reader is referred to the web version of this article.)

role in the development of the stress heterogeneity at low levels of deformation (prior to twin activation). It is worth noting that the experimental analysis has been performed on pure Mg, with a relatively low threshold stress for basal slip (around 3.3 MPa [48]), while a higher value (11 MPa) was used in the simulations to represent the hardening effect on basal slip in typical rare-earth-free Mg alloys. It is reasonable to infer that the easier activation of basal slip in pure Mg can result in stronger stress heterogeneity than in Mg alloys, especially at the early stage of deformation, which may in turn increase the propensity of low Schmid factor twins. This is further reflected by the fact that the suppression of basal slip during plastic deformation even completely suppressed the twin formation with a Schmid factor smaller than 0.2 (red curve in Fig. 6(d)). Moreover, the statistical analysis on deformed Zr, based on EBSD characterisation [83], was also given in Fig. 6(d). It can be seen that the propensity to activate low Schmid factor twins in Zr was much lower than in pure Mg. Again, this can be partly ascribed to the 'harder' slip modes in Zr compared to Mg. In addition, the predicted propensity of twin transmission across GBs was also compared to the EBSD measurements on pure Mg, as shown in Fig. 6(e). It is clear that the predicted tendency agreed well with the experimental observations, where twin transmission most frequently occurred at GBs with low misorientation angles, and the fraction dropped substantially to nearly zero once the misorientation angle reached roughly 50° and higher [83,88].

As shown in Fig. 8, the development of the grain-level stress predicted in the current work was compared to experimental results from an AZ31 Mg alloy, obtained by three-dimensional synchrotron X-ray diffraction [84]. It is worth noting that only the average values for each population from the experiments were

included in Fig. 8 for the sake of brevity. Both simulations and experiments suggest that the average resolved shear stress within the twins was very close to that developed within the parents. It should be noted that a lower magnitude of average stress was observed in the experiments than in the simulations. This can be ascribed to the different macroscopic loading conditions, where the experiment was performed at a strain of 0.3% with a low macroscopic stress of 54 MPa, while the simulation result corresponded to a condition at a strain of 5% with a loading stress of 120 MPa. Moreover, we have qualitatively compared the load sharing within twins and parents obtained from the synchrotron X-ray diffraction experiment on Zr [85] with the current simulation without consideration of dislocation-induced plasticity. As the practically available slip systems in Zr are relatively harder than those in Mg, much less dislocation accommodation would be expected accompanying twin formation in Zr. As shown in Fig. 8(c), both simulations and experiments show that the retardation of dislocation accommodation can induce the generation of high back-stresses during twin formation, *i.e.* the shear stress developed within twins was substantially lower than that within the associated parent regions.

4.2. Effect of dislocation accommodation on deformation twinning

Section 3 clearly demonstrates that dislocation accommodation plays a critical role not only for the morphological characteristics of tension twins but also for the local stress redistribution within twins and their parent crystals. This fact, in turn, evidently affects the mechanical properties of Mg, including the underlying deformation mechanisms and collective polycrystal strain hardening effects that lead to the material's overall strength and ductility response. It has been reported that emissary slip structures generally occurred in the matrix ahead of terminating twins, such as in body centered cubic Mo alloys [89] and face centered cubic Fe alloys [90], respectively. In recent studies, similar studies on the plastic relaxation of the stress concentration developed close to tension twins in Mg alloys have been performed, showing kink bands and emissary $\langle a \rangle$ and $\langle a+c \rangle$ dislocation slip patterns in the vicinity of tension twins in pure Mg [91] and a Mg-Y alloy [92]. Our current full-field simulations also revealed profuse basal dislocations in the matrix surrounding tension twin tips, as shown in Figs. 1, 3 and 5. We observed that the pronounced activation of basal dislocations has caused a strong stress relaxation effect (from around 240 MPa to 175 MPa) in the vicinity of twin tips, which, in turn, dramatically reduced the driving force for twin propagation. This can to some extent explain the fact that much narrower deformation twins are usually formed in Zr than in Mg [25,37]. Due to the relatively harder slip systems in Zr compared to Mg, the formation of deformation twins in Zr is mainly accommodated by elastic strain in the surrounding matrix, which induces strong stress concentration near the twin tips, and subsequently facilitates rapid twin propagation throughout the grain.

Both the current simulations (Sections 3.2 and 3.3) and the experimental measurements on Mg single crystals [19,22] have revealed that twin-twin interactions in Mg can effectively improve the material's strength through hampering twin propagation and thickening. For example, Fig. 1(e) indicates that the applied stress for twin growth (at 1.5% strain) was enhanced to 80 MPa when containing cozone twin-twin interactions, compared to 50 MPa for a single twin variant. Furthermore, a Bauschinger effect was observed for the cyclic deformation of a Mg single crystal containing two activated twin systems, where the loading stress required for twin growth after the formation of twin intersections was much higher than that required for detwinning during the reverse loading step, being 90 MPa relative to 62 MPa (Fig. 2). A symmetrical stress-strain hysteresis loop was instead predicted for the single crystal only containing a single twin variant. Since the short-range effects, *i.e.* the directionality of mobile dislocations in their resistance to glide or the annihilation of dislocations during reverse loading, were not considered in the current model, the simulated Bauschinger effect can be ascribed to inhomogeneous plastic flow and long-range effects, such as the back-stress arising from the hindrance of twin propagation and growth by twin networks. The quantitative assessment of the shear stress distribution in Mg single crystals (Fig. 2) implies that twin-twin interaction can lead to substantial stress inhomogeneity in both parent and twin crystals. These intense stress variations induced by twin-twin interactions did not vanish upon unloading and even persisted upon the detwinning-dominated reverse loading stage.

In addition to the stress heterogeneity, the formation of twin networks would necessarily cause an additional back-stress due to the large strain misfit between the sheared twin and the unsheared parent domains. This large back-stress would oppose the local thickening of the twin boundary and thus provide a strong energy penalty against twin growth. It is expected that the easy activation of basal slips can effectively accommodate the strain incompatibility and relax the stress partitioning between parents and twins arising from twin-twin interactions. Hence, basal dislocation accommodation can diminish the twin-twin interaction induced strengthening effect in Mg. This is revealed by the reduction of both the macroscopic stress (180 MPa compared to 140 MPa) and the back-stress within the domain (86 MPa compared to 14 MPa) when basal slip was involved to accommodate the strain incompatibility (Fig. 4). In addition, the activation of basal dislocations can profoundly reduce the stress concentration at the intersection of two twins (a drop from 320 MPa to 170 MPa as shown in Fig. 4). This plastic relaxation of the localised stress can thus effectively hamper crack initiation near twin-twin intersections. This effect can rationalize the experimental observations that the twin mesh configuration in a Mg–Li alloy did not lead to premature failure [9,29]. In summary, the impact of dislocation accommodation on twin-twin interactions is twofold. Dislocation accommodation can diminish the twin-twin interaction induced strengthening effect in Mg by relieving the stress partitioning between twins and parents, *i.e.* the development of back-stresses, whereas the activation of basal dislocations can effectively relax stress concentrations in the vicinity of twin junctions and can thus alleviate crack nucleation and improve the materials' ductility.

4.3. Strong grain neighbourhood effect on local plastic deformation

In general, the anomalous twinning behaviour, *i.e.* the absence of high Schmid factor twins and the presence of low Schmid factor twins, can be attributed to the large deviation of the local stress in a grain from the applied stress, which is induced by the plastic anisotropy and the local constraints prescribed by different sets of neighbouring grains. This is supported by the statistical analysis of the stress distribution at the grain scale shown in Fig. 7, which shows that the grain-averaged shear stress for a twin system increased proportionally with an increase in the twin Schmid factor, however, a large scatter in the correlation can be observed even at a low level of deformation (0.5%). It is worth noting that the formation of low Schmid factor twins was instead not observed when dislocation accommodation was inhibited. This suggests that the different basal slip activity for each grain, depending on both its own orientation and surrounding grains, produced the observed stress heterogeneity at initial low levels of deformation. As presented in Fig. 10(b) and (c), the formation of low Schmid factor twins was associated with the strong stress concentration near GBs, induced by the accumulation of basal dislocations in the adjoining grain. This high stress was mainly concentrated near GBs and decayed when approaching the grain interior. Therefore, with increasing strain, these low Schmid factor twins were

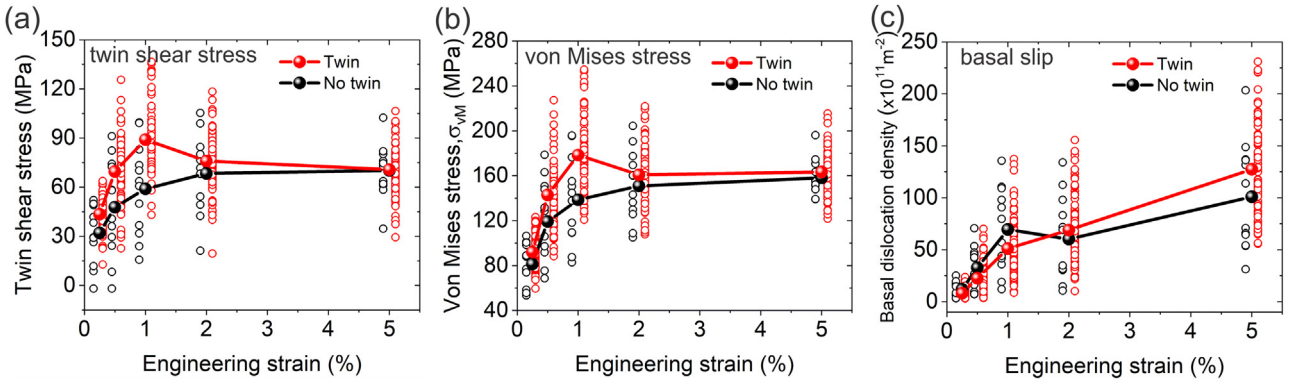

Fig. 12. Comparison of the stress development and basal slip activity in the grains with and without twin formation (twin Schmid factors higher than 0.4). Evolution of the twin resolved shear stress (a), von Mises stress (b), and basal dislocation density (c) with increasing applied strain. Open circles represent the result for an individual grain. Solid circles depict the average value for each population.

arrested within the grain interior and exhibited a relatively small size. The statistical analysis in Fig. 7 also suggests that, on average, the twin volume fraction was relatively low in a grain when it was less stressed. These low Schmid factor twins were thus usually activated to accommodate the local strain incompatibility rather than the macroscopic strain.

Section 3.4.3 shows that the absence of high Schmid factor twins was generally related to the load sharing among grains. These grains were usually close to large basal slip bands across multiple grains. That is, the applied strain was preferentially accommodated by their plastically soft neighbours, especially those along the loading direction, which subsequently resulted in stress relaxation and impediment of twin formation within such grains. Fig. 12 shows the statistical analysis on grains with high twin Schmid factors (above 0.4). Fig. 12(a) and (b) indicate that, up to 2% strain, both the average twin resolved shear stress and the von Mises stress developed in grains with twin formation were significantly higher than those without twin formation, albeit with a large scatter among individual grains. The largest difference in the stress development occurred at a strain of 1%, which corresponded to the twin activation stage. Despite the distinct difference in the stress development, a similar amount of basal slip activity was observed in these two groups (up to 5% strain), as shown in Fig. 12(c). This again implies the remarkable role of the basal slip activity within the neighbouring grains, in addition to the plastic properties of the grain itself, in determining the activation of deformation twins. These findings show that the local plastic deformation mechanisms for an individual grain can be complex and are strongly influenced by the plastic behaviour of the near- and far-field crystal neighbourhood. Hence, the macroscopic Schmid factor alone or the geometric compatibility factor alone, depending on the crystallography of the grain itself or the nearest neighbour grain, can usually not precisely predict the twinning behaviour.

5. Conclusions

This work has presented a microstructure-sensitive and spatially resolved mechanical model within a finite strain framework capable of describing the concurrent dislocation slip- and deformation twinning-induced plasticity in a polycrystal. A dislocation density-based crystal plasticity model was employed to describe the dislocation activity and the distribution of stress and strain. This constitutive model was integrated with a multi-phase-field model to predict the propagation and growth of deformations twins and twin-twin interactions. The coupled model can help rationalizing the local plastic deformation mechanisms and the associated mechanical behaviour of hcp metals.

The developed model has been employed to investigate the complex twinning-detwinning behaviour, the interaction of dislocations, twins and GBs, and the strong grain neighbour effect in Mg single crystal and polycrystals during large monotonic and cyclic deformation. It was found that both cozone and non-cozone twin-twin intersections can act as barriers to impede twin propagation and growth, producing an effective strengthening effect. The intense stress variation induced by twin-twin interactions did not vanish upon unloading and even persisted during the detwinning-dominated reverse loading stage. The impact of dislocation slip on twin-twin interactions is found to be twofold. Dislocation accommodation can diminish the twin-twin interaction induced strengthening effect in Mg by relieving the stress partitioning between twins and parents, *i.e.* the development of back-stresses, whereas it can effectively relax the stress concentration near twin junctions and thus may alleviate crack nucleation and improve the materials' ductility. The statistical analysis of the stress distribution at the grain scale in the Mg polycrystal suggests that, on average, grain-averaged shear stress for twinning increased proportionally with an increase in twin Schmid factor, however, there was a large scatter in the correlation even at low levels of deformation (0.5%). Moreover, the inhibition of dislocation accommodation has resulted in the absence of low Schmid factor twins. Basal slip-induced plastic anisotropy in each grain and the constraints imposed by the local boundary conditions were found to induce a profound stress heterogeneity among the grains at low levels of deformation. It has been shown that deformation twins were relatively small in less-stressed grains, which means that low Schmid factor twins were usually activated to accommodate the local strain incompatibility rather than the macroscopic strain. In addition, grains with high twin Schmid factors, yet without twin formation, were generally located in the vicinity of large slip bands across multiple grains. The reason for this effect is that the macroscopic strain was preferentially accommodated by their plastically soft neighbours, especially those along the loading direction, which subsequently resulted in stress relaxation and impediment of twin formation within such grains.

Declaration of Competing Interest

The authors declare that they have no known competing financial interests or personal relationships that could have appeared to influence the work reported in this paper.

Acknowledgements

The authors acknowledge financial support by the Deutsche Forschungsgemeinschaft (DFG) within projects A01 and C01 of the Collaborative Research Center (SFB) 1394 "Structural and Chemical Atomic Complexity - from defect phase diagrams to material properties", project ID 409476157. C.L. also gratefully acknowledges the support from Shanghai Jiao Tong University.

Appendix A. Notation

As a general scheme of notation, vectors are written as boldface lowercase letters (*e.g.* **a**, **b**), second-order tensors as boldface capital letters (*e.g.* **A**, **B**), and fourth-order tensors as blackboard-bold capital letters (*e.g.* $\mathbb{A}$, $\mathbb{B}$). For vectors and tensors, Cartesian components are denoted as, respectively, a_i, A_{ij} and A_{ijkl}. Second-order tensors are represented in this work as linear mappings between vectors and are denoted as **Ab** (in components $A_{ij}b_j$, implicit summation over repeated indices is used unless specified otherwise) and, likewise, fourth-order tensors represent linear mappings between second-orders and are designated as $\mathbb{A}\mathbf{B}$ ($A_{ijkl}B_{kl}$). The composition of two second-order tensors is denoted as **AB** ($A_{ik}B_{kj}$). The tensor (or dyadic) product between two vectors is denoted as $\mathbf{a} \otimes \mathbf{b}$ ($a_i b_j$). All inner products are indicated by a single dot between the tensorial quantities of the same order, *e.g.* $\mathbf{a} \cdot \mathbf{b}$ ($a_i b_i$) for vectors and $\mathbf{A} \cdot \mathbf{B}$ ($A_{ij}B_{ij}$) for second-order tensors. The transpose, $\mathbf{A}^{\mathrm{T}}$, of a tensor **A** is denoted by a superscript "T", and the inverse, $\mathbf{A}^{-1}$, by a superscript "-1". Additional notation is introduced where required.

Supplementary material

Supplementary material associated with this article can be found, in the online version, at doi:10.1016/j.actamat.2022.118444

References

[1] M. Yoo, Slip, twinning, and fracture in hexagonal close-packed metals, Metall. Trans. A 12 (3) (1981) 409–418.
[2] M. Barnett, Twinning and the ductility of magnesium alloys: part I:"tension" twins, Mater. Sci. Eng. 464 (1–2) (2007) 1–7.
[3] L. Wu, A. Jain, D. Brown, G. Stoica, S. Agnew, B. Clausen, D. Fielden, P. Liaw, Twinning–detwinning behavior during the strain-controlled low-cycle fatigue testing of a wrought magnesium alloy, ZK60A, Acta Mater. 56 (4) (2008) 688–695.
[4] S.R. Agnew, Ö. Duygulu, Plastic anisotropy and the role of non-basal slip in magnesium alloy AZ31B, Int. J. Plast. 21 (6) (2005) 1161–1193.
[5] C. Bettles, M. Barnett, Advances in Wrought Magnesium Alloys: Fundamentals of Processing, Properties and Applications, Elsevier, 2012.
[6] M. Ritzo, R. Lebensohn, L. Capolungo, S. Agnew, Accounting for the effect of dislocation climb-mediated flow on the anisotropy and texture evolution of Mg alloy, AZ31B, Mater. Sci. Eng. 839 (2022) 142581.
[7] J. Bohlen, M.R. Nürnberg, J.W. Senn, D. Letzig, S.R. Agnew, The texture and anisotropy of magnesium–zinc–rare earth alloy sheets, Acta Mater. 55 (6) (2007) 2101–2112.
[8] J.F. Nie, Y. Zhu, J. Liu, X.-Y. Fang, Periodic segregation of solute atoms in fully coherent twin boundaries, Science 340 (6135) (2013) 957–960.
[9] M. Lentz, M. Risse, N. Schaefer, W. Reimers, I. Beyerlein, Strength and ductility with $\{1\,0\,\bar{1}\,1\}$ $\{1\,0\,\bar{1}\,2\}$ double twinning in a magnesium alloy, Nat. Commun. 7 (1) (2016) 1–7.
[10] B.-Y. Liu, F. Liu, N. Yang, X.-B. Zhai, L. Zhang, Y. Yang, B. Li, J. Li, E. Ma, J.-F. Nie, et al., Large plasticity in magnesium mediated by pyramidal dislocations, Science 365 (6448) (2019) 73–75.
[11] Z. Wu, W. Curtin, The origins of high hardening and low ductility in magnesium, Nature 526 (7571) (2015) 62–67.
[12] S. Sandlöbes, M. Friák, S. Zaefferer, A. Dick, S. Yi, D. Letzig, Z. Pei, L.-F. Zhu, J. Neugebauer, D. Raabe, The relation between ductility and stacking fault energies in Mg and Mg–Y alloys, Acta Mater. 60 (6–7) (2012) 3011–3021.
[13] T. Trang, J. Zhang, J. Kim, A. Zargaran, J. Hwang, B.-C. Suh, N. Kim, Designing a magnesium alloy with high strength and high formability, Nat. Commun. 9 (1) (2018) 1–6.
[14] Z. Wu, R. Ahmad, B. Yin, S. Sandlöbes, W. Curtin, Mechanistic origin and prediction of enhanced ductility in magnesium alloys, Science 359 (6374) (2018) 447–452.
[15] N. Stanford, D. Atwell, M.R. Barnett, The effect of Gd on the recrystallisation, texture and deformation behaviour of magnesium-based alloys, Acta Mater. 58 (20) (2010) 6773–6783.
[16] L. Zhao, B. Guan, Y. Xin, X. Huang, C. Liu, P. Wu, Q. Liu, A quantitative study on mechanical behavior of Mg alloys with bimodal texture components, Acta Mater. 214 (2021) 117013.
[17] J. Wang, M.R.G. Ferdowsi, S.R. Kada, S. Babaniaris, B. Hutchinson, P.A. Lynch, M.R. Barnett, Appearance of textures with a *c*-axis parallel to the extrusion direction in Mg alloys, Scr. Mater. 210 (2022) 114422.
[18] M.-T. Pérez-Prado, J. Bohlen, S. Yi, D. Letzig, T. Al-Samman, J. Robson, M. Barnett, W. Poole, C. Mendis, S. Agnew, et al., Emerging hot topics and research questions in wrought magnesium alloy development, JOM 72 (7) (2020) 2561–2567.
[19] Q. Yu, J. Wang, Y. Jiang, R.J. McCabe, N. Li, C.N. Tomé, Twin–twin interactions in magnesium, Acta Mater. 77 (2014) 28–42.
[20] M. Gong, S. Xu, Y. Jiang, Y. Liu, J. Wang, Structural characteristics of $\{\bar{1}012\}$ non-cozone twin-twin interactions in magnesium, Acta Mater. 159 (2018) 65–76.
[21] M.A. Kumar, M. Gong, I. Beyerlein, J. Wang, C.N. Tomé, Role of local stresses on co-zone twin-twin junction formation in HCP magnesium, Acta Mater. 168 (2019) 353–361.
[22] Q. Yu, Y. Jiang, J. Wang, Tension-compression-tension tertiary twins in coarse–grained polycrystalline pure magnesium at room temperature, Philos. Mag. Lett. 95 (4) (2015) 194–201.
[23] H. El Kadiri, J. Kapil, A. Oppedal, L. Hector Jr., S.R. Agnew, M. Cherkaoui, S. Vogel, The effect of twin–twin interactions on the nucleation and propagation of {10-12} twinning in magnesium, Acta Mater. 61 (10) (2013) 3549–3563.
[24] Q. Yu, Y. Jiang, J. Wang, Cyclic deformation and fatigue damage in single-crystal magnesium under fully reversed strain-controlled tension–compression in the [10-10] direction, Scr. Mater. 96 (2015) 41–44.
[25] P.-A. Juan, C. Pradalier, S. Berbenni, R. McCabe, C. Tomé, L. Capolungo, A statistical analysis of the influence of microstructure and twin–twin junctions on twin nucleation and twin growth in Zr, Acta Mater. 95 (2015) 399–410.
[26] M. Koyama, E. Akiyama, K. Tsuzaki, D. Raabe, Hydrogen-assisted failure in a twinning-induced plasticity steel studied under in situ hydrogen charging by electron channeling contrast imaging, Acta Mater. 61 (12) (2013) 4607–4618.
[27] C.A. Stein, A. Cerrone, T. Ozturk, S. Lee, P. Kenesei, H. Tucker, R. Pokharel, J. Lind, C. Hefferan, R.M. Suter, et al., Fatigue crack initiation, slip localization and twin boundaries in a nickel-based superalloy, Curr. Opin. Solid State Mater. Sci. 18 (4) (2014) 244–252.
[28] S. Zhao, R. Zhang, Q. Yu, J. Ell, R.O. Ritchie, A.M. Minor, Cryoforged nanotwinned titanium with ultrahigh strength and ductility, Science 373 (6561) (2021) 1363–1368.
[29] X. Wang, L. Jiang, C. Cooper, K. Yu, D. Zhang, T.J. Rupert, S. Mahajan, I.J. Beyerlein, E.J. Lavernia, J.M. Schoenung, Toughening magnesium with gradient twin meshes, Acta Mater. 195 (2020) 468–481.
[30] H. Abdolvand, J. Wright, A.J. Wilkinson, Strong grain neighbour effects in polycrystals, Nat. Commun. 9 (1) (2018) 1–11.
[31] M. Arul Kumar, B. Clausen, L. Capolungo, R. McCabe, W. Liu, J. Tischler, C. Tome, Deformation twinning and grain partitioning in a hexagonal close-packed magnesium alloy, Nat. Commun. 9 (1) (2018) 1–8.
[32] A. Jamali, A. Ma, J. LLorca, Influence of grain size and grain boundary misorientation on the fatigue crack initiation mechanisms of textured AZ31 Mg alloy, Scr. Mater. 207 (2022) 114304.
[33] Y. Xu, S. Joseph, P. Karamched, K. Fox, D. Rugg, F.P. Dunne, D. Dye, Predicting dwell fatigue life in titanium alloys using modelling and experiment, Nat. Commun. 11 (1) (2020) 1–13.
[34] M.P. Puls, The Effect of Hydrogen and Hydrides on the Integrity of Zirconium Alloy Components: Delayed Hydride Cracking, Springer Science & Business Media, 2012.
[35] Y. Guo, H. Abdolvand, T. Britton, A. Wilkinson, Growth of $\{11\bar{2}2\}$ twins in titanium: acombined experimental and modelling investigation of the local state of deformation, Acta Mater. 126 (2017) 221–235.
[36] Y. Guo, T. Britton, A. Wilkinson, Slip band–grain boundary interactions in commercial-purity titanium, Acta Mater. 76 (2014) 1–12.
[37] I. Beyerlein, L. Capolungo, P. Marshall, R. McCabe, C. Tomé, Statistical analyses of deformation twinning in magnesium, Philos. Mag. 90 (16) (2010) 2161–2190.
[38] M.A. Kumar, M. Wroński, R.J. McCabe, L. Capolungo, K. Wierzbanowski, C.N. Tomé, Role of microstructure on twin nucleation and growth in HCP titanium: a statistical study, Acta Mater. 148 (2018) 123–132.
[39] C. Liu, P. Shanthraj, M. Diehl, F. Roters, S. Dong, J. Dong, W. Ding, D. Raabe, An integrated crystal plasticity–phase field model for spatially resolved twin nucleation, propagation, and growth in hexagonal materials, Int. J. Plast. 106 (2018) 203–227.
[40] C. Liu, P. Shanthraj, J.D. Robson, M. Diehl, S. Dong, J. Dong, W. Ding, D. Raabe, On the interaction of precipitates and tensile twins in magnesium alloys, Acta Mater. 178 (2019) 146–162.
[41] M. Ardeljan, R.J. McCabe, I.J. Beyerlein, M. Knezevic, Explicit incorporation of deformation twins into crystal plasticity finite element models, Comput. Methods Appl. Mech. Eng. 295 (2015) 396–413.
[42] J. Cheng, S. Ghosh, Crystal plasticity finite element modeling of discrete twin evolution in polycrystalline magnesium, J. Mech. Phys. Solids 99 (2017) 512–538.
[43] H. Qiao, M. Barnett, P. Wu, Modeling of twin formation, propagation and growth in a Mg single crystal based on crystal plasticity finite element method, Int. J. Plast. 86 (2016) 70–92.
[44] S.A. Chester, J.V. Bernier, N.R. Barton, L. Balogh, B. Clausen, J.K. Edmiston, Direct numerical simulation of deformation twinning in polycrystals, Acta Mater. 120 (2016) 348–363.

[45] C. Mareau, M.R. Daymond, Micromechanical modelling of twinning in polycrystalline materials: application to magnesium, Int. J. Plast. 85 (2016) 156–171.
[46] C. Tomé, R.A. Lebensohn, U. Kocks, A model for texture development dominated by deformation twinning: application to zirconium alloys, Acta Metall. Mater. 39 (11) (1991) 2667–2680.
[47] R.A. Lebensohn, C. Tomé, A self-consistent anisotropic approach for the simulation of plastic deformation and texture development of polycrystals: application to zirconium alloys, Acta Metall. Mater. 41 (9) (1993) 2611–2624.
[48] I. Beyerlein, R. McCabe, C. Tomé, Effect of microstructure on the nucleation of deformation twins in polycrystalline high-purity magnesium: a multi-scale modeling study, J. Mech. Phys. Solids 59 (5) (2011) 988–1003.
[49] H. Wang, P. Wu, J. Wang, C. Tomé, A crystal plasticity model for hexagonal close packed (HCP) crystals including twinning and de-twinning mechanisms, Int. J. Plast. 49 (2013) 36–52.
[50] S.R. Kalidindi, Incorporation of deformation twinning in crystal plasticity models, J. Mech. Phys. Solids 46 (2) (1998) 267–290.
[51] H. Abdolvand, M. Majkut, J. Oddershede, J.P. Wright, M.R. Daymond, Study of 3-D stress development in parent and twin pairs of a hexagonal close-packed polycrystal: part II–crystal plasticity finite element modeling, Acta Mater. 93 (2015) 235–245.
[52] F. Roters, M. Diehl, P. Shanthraj, P. Eisenlohr, C. Reuber, S.L. Wong, T. Maiti, A. Ebrahimi, T. Hochrainer, H.-O. Fabritius, et al., Damask–the Düsseldorf advanced material simulation kit for modeling multi-physics crystal plasticity, thermal, and damage phenomena from the single crystal up to the component scale, Comput. Mater. Sci 158 (2019) 420–478.
[53] A.G. Khachaturyan, Theory of Structural Transformations in Solids, Courier Corporation, 2013.
[54] L.-Q. Chen, Phase-field models for microstructure evolution, Annu. Rev. Mater. Res. 32 (1) (2002) 113–140.
[55] I. Steinbach, M. Apel, Multi phase field model for solid state transformation with elastic strain, Phys. D 217 (2) (2006) 153–160.
[56] N. Moelans, B. Blanpain, P. Wollants, An introduction to phase-field modeling of microstructure evolution, Calphad 32 (2) (2008) 268–294.
[57] Y. Wang, J. Li, Phase field modeling of defects and deformation, Acta Mater. 58 (4) (2010) 1212–1235.
[58] P. Shanthraj, L. Sharma, B. Svendsen, F. Roters, D. Raabe, A phase field model for damage in elasto-viscoplastic materials, Comput. Methods Appl. Mech. Eng. 312 (2016) 167–185.
[59] P. Shanthraj, B. Svendsen, L. Sharma, F. Roters, D. Raabe, Elasto-viscoplastic phase field modelling of anisotropic cleavage fracture, J. Mech. Phys. Solids 99 (2017) 19–34.
[60] P. Shanthraj, C. Liu, A. Akbarian, B. Svendsen, D. Raabe, Multi-component chemo-mechanics based on transport relations for the chemical potential, Comput. Methods Appl. Mech. Eng. 365 (2020) 113029.
[61] C. Liu, A. Garner, H. Zhao, P.B. Prangnell, B. Gault, D. Raabe, P. Shanthraj, CALPHAD-informed phase-field modeling of grain boundary microchemistry and precipitation in Al-Zn-Mg-Cu alloys, Acta Mater. 214 (2021) 116966.
[62] C. Liu, A. Davis, J. Fellowes, P.B. Prangnell, D. Raabe, P. Shanthraj, CALPHAD-informed phase-field model for two-sublattice phases based on chemical potentials: η-phase precipitation in Al-Zn-Mg-Cu alloys, Acta Mater. 226 (2022) 117602.
[63] S. Hu, C.H. Henager Jr., L. Chen, Simulations of stress-induced twinning and de-twinning: a phase field model, Acta Mater. 58 (19) (2010) 6554–6564.
[64] J.D. Clayton, J. Knap, A phase field model of deformation twinning: nonlinear theory and numerical simulations, Phys. D 240 (9–10) (2011) 841–858.
[65] H. Liu, F. Lin, P. Zhao, N. Moelans, Y. Wang, J. Nie, Formation and autocatalytic nucleation of co-zone $\{1\,0\,\bar{1}\,2\}$ deformation twins in polycrystalline Mg: a phase field simulation study, Acta Mater. 153 (2018) 86–107.
[66] X. Hu, Y. Ji, T.W. Heo, L.-Q. Chen, X. Cui, Phase-field model of deformation twin-grain boundary interactions in hexagonal systems, Acta Mater. 200 (2020) 821–834.
[67] R. Kondo, Y. Tadano, K. Shizawa, A phase-field model of twinning and detwinning coupled with dislocation-based crystal plasticity for HCP metals, Comput. Mater. Sci 95 (2014) 672–683.
[68] N. Grilli, A.C. Cocks, E. Tarleton, A phase field model for the growth and characteristic thickness of deformation-induced twins, J. Mech. Phys. Solids 143 (2020) 104061.
[69] X. Hu, Y. Ji, L. Chen, R.A. Lebensohn, L.-Q. Chen, X. Cui, Spectral phase–field model of deformation twinning and plastic deformation, Int. J. Plast. 143 (2021) 103019.
[70] G. Liu, H. Mo, J. Wang, Y. Shen, Coupled crystal plasticity finite element-phase field model with kinetics-controlled twinning mechanism for hexagonal metals, Acta Mater. 202 (2021) 399–416.
[71] M. Rezaee-Hajidehi, P. Sadowski, S. Stupkiewicz, Deformation twinning as a displacive transformation: finite-strain phase-field model of coupled twinning and crystal plasticity, J. Mech. Phys. Solids (2022) 104855.
[72] P. Zhao, T.S.E. Low, Y. Wang, S.R. Niezgoda, Finite strain phase-field microelasticity theory for modeling microstructural evolution, Acta Mater. 191 (2020) 253–269.
[73] A. Finel, Y. Le Bouar, A. Gaubert, U. Salman, Phase field methods: microstructures, mechanical properties and complexity, C.R. Phys. 11 (3–4) (2010) 245–256.
[74] J. Hamma, B. APPOLAIRE, Y. Le Bouar, A. Finel, Phase field modeling of deformation twinning in β-metastable titanium alloys, in: MATEC Web of Conferences, vol. 321, EDP Sciences, 2020, p. 12026.
[75] E. Orowan, Zur kristallplastizität. i, Z. Phys. 89 (9) (1934) 605–613.
[76] K. Tuma, S. Stupkiewicz, H. Petryk, Rate-independent dissipation in phase–field modelling of displacive transformations, J. Mech. Phys. Solids 114 (2018) 117–142.
[77] P. Song, T. Yang, Y. Ji, Z. Wang, Z. Yang, L. Chen, L. Chen, A comparison of fourier spectral iterative perturbation method and finite element method in solving phase-field equilibrium equations, Commun. Comput. Phys. 21 (5) (2017) 1325–1349.
[78] P. Eisenlohr, M. Diehl, R.A. Lebensohn, F. Roters, A spectral method solution to crystal elasto-viscoplasticity at finite strains, Int. J. Plast. 46 (2013) 37–53.
[79] S. Balay, S. Abhyankar, M.F. Adams, S. Benson, J. Brown, P. Brune, K. Buschelman, E. Constantinescu, L. Dalcin, A. Dener, V. Eijkhout, W.D. Gropp, V. Hapla, T. Isaac, P. Jolivet, D. Karpeev, D. Kaushik, M.G. Knepley, F. Kong, S. Kruger, D.A. May, L.C. McInnes, R.T. Mills, L. Mitchell, T. Munson, J.E. Roman, K. Rupp, P. Sanan, J. Sarich, B.F. Smith, S. Zampini, H. Zhang, H. Zhang, J. Zhang, PETSc/TAO Users Manual, Technical Report, Argonne National Laboratory, 2022.
[80] S.J. Benson, T.S. Munson, Flexible complementarity solvers for large-scale applications, Optim. Methods Softw. 21 (1) (2006) 155–168.
[81] S. Stupkiewicz, H. Petryk, A robust model of pseudoelasticity in shape memory alloys, Int. J. Numer. Methods Eng. 93 (7) (2013) 747–769.
[82] M. Arul Kumar, I.J. Beyerlein, R.J. McCabe, C.N. Tome, Grain neighbour effects on twin transmission in hexagonal close-packed materials, Nat. Commun. 7 (1) (2016) 1–9.
[83] L. Capolungo, P. Marshall, R. McCabe, I. Beyerlein, C. Tomé, Nucleation and growth of twins in Zr: a statistical study, Acta Mater. 57 (20) (2009) 6047–6056.
[84] K. Louca, H. Abdolvand, C. Mareau, M. Majkut, J. Wright, Formation and annihilation of stressed deformation twins in magnesium, Commun. Mater. 2 (1) (2021) 1–11.
[85] H. Abdolvand, K. Louca, C. Mareau, M. Majkut, J. Wright, On the nucleation of deformation twins at the early stages of plasticity, Acta Mater. 196 (2020) 733–746.
[86] D. Raabe, M. Sachtleber, Z. Zhao, F. Roters, S. Zaefferer, Micromechanical and macromechanical effects in grain scale polycrystal plasticity experimentation and simulation, Acta Mater. 49 (17) (2001) 3433–3441.
[87] Z. Zhao, M. Ramesh, D. Raabe, A. Cuitino, R. Radovitzky, Investigation of three--dimensional aspects of grain-scale plastic surface deformation of an aluminum oligocrystal, Int. J. Plast. 24 (12) (2008) 2278–2297.
[88] T. Bieler, P. Eisenlohr, F. Roters, D. Kumar, D. Mason, M. Crimp, D. Raabe, The role of heterogeneous deformation on damage nucleation at grain boundaries in single phase metals, Int. J. Plast. 25 (9) (2009) 1655–1683.
[89] S. Mahajan, Interrelationship between slip and twinning in BCC crystals, Acta Metall. 23 (6) (1975) 671–684.
[90] S. Mahajan, G. Chin, Formation of deformation twins in fcc crystals, Acta Metall. 21 (10) (1973) 1353–1363.
[91] E. Roberts, P. Partridge, The accommodation around $\{1\,0\,\bar{1}\,2\}\langle 1\,0\,\bar{1}\,1\rangle$ twins in magnesium, Acta Metall. 14 (4) (1966) 513–527.
[92] K. Yaddanapudi, B. Leu, M.A. Kumar, X. Wang, J.M. Schoenung, E.J. Lavernia, T.J. Rupert, I.J. Beyerlein, S. Mahajan, Accommodation and formation of $\{1\,0\,\bar{1}\,2\}$ twins in Mg-Y alloys, Acta Mater. 204 (2021) 116514.